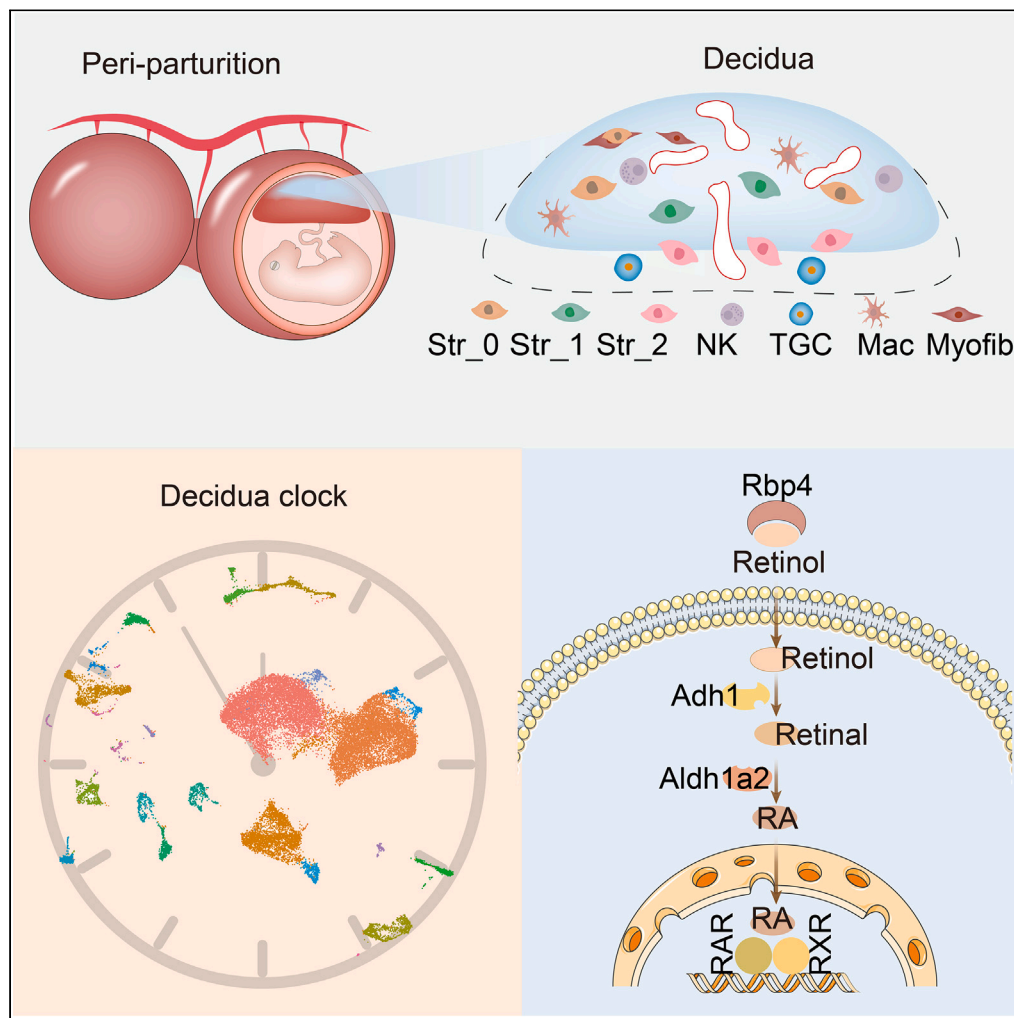


Article

Stromal cells-specific retinoic acid determines parturition timing at single-cell and spatial-temporal resolution



Hui Zhao, Yang Wang, Hui Xu, ..., Haili Bao, Haibin Wang, Wenbo Deng

haili_bao@163.com (H.B.)
haibin.wang@vip.163.com (H.W.)
wbdeng@xmu.edu.cn (W.D.)

Highlights

Stromal cells are the most abundant cell type in mice decidua

RA is a potential decidua critical factor for labor onset

RA participates in parturition by regulating ECM genes

Stromal cells dominate the complex interactions with other cell types

Zhao et al., iScience 26, 107796
October 20, 2023 © 2023 The Author(s).
<https://doi.org/10.1016/j.isci.2023.107796>



Article

Stromal cells-specific retinoic acid determines parturition timing at single-cell and spatial-temporal resolution

Hui Zhao,^{1,2,6} Yang Wang,^{1,2,6} Hui Xu,^{1,2,4,6} Meng Liu,^{1,2} Xinmei Xu,^{1,2} Sijing Zhu,^{1,2} Zhao Liu,^{1,2,5} Han Cai,^{1,2} Yinan Wang,^{1,2} Jinhua Lu,^{1,2} Xiaoqing Yang,³ Shuangbo Kong,^{1,2} Haili Bao,^{1,2,*} Haibin Wang,^{1,2,*} and Wenbo Deng^{1,2,7,*}

SUMMARY

The underlying mechanisms governing parturition remain largely elusive due to limited knowledge of parturition preparation and initiation. Accumulated evidences indicate that maternal decidua plays a critical role in parturition initiation. To comprehensively decrypt the cell heterogeneity in decidua approaching parturition, we investigate the roles of various cell types in mouse decidua process and reveal previously unappreciated insights in parturition initiation utilizing single-cell RNA sequencing (scRNA-seq). We enumerate the cell types in decidua and identity five different stromal cells populations and one decidualized stromal cells. Furthermore, our study unravels that stromal cells prepare for parturition by regulating local retinol acid (RA) synthesis. RA supplement decreases expression of extracellular matrix-related genes *in vitro* and accelerates the timing of parturition *in vivo*. Collectively, the discovery of contribution of stromal cells in parturition expands current knowledge about parturition and opens up avenues for the intervention of preterm birth (PTB).

INTRODUCTION

Parturition initiation is orchestrated by multiple mechanisms, while our understanding about this process is significantly behind. Timely parturition is critical for the survival of the neonates and their future health trajectory.^{1,2} Parturition initiation is elegantly directed, which requires adequate preparation under the coordination of maternal decidua, placenta, and fetus.³ However, the developmental and physiological mechanisms governing parturition remain unsolved mysteries as relatively little is known about the processes of parturition preparation and initiation, making combating against preterm birth (PTB) a formidable challenge.⁴

Accumulating data suggest that “decidual clock” is critical for parturition initiation as evidenced by the two-hit hypothesis: genetic predispose and environmental stimulus.^{3,5–9} Additionally, the prevailing hypothesis about the role of decidua in parturition is that the decidua originated prostaglandin F2 alpha (PGF2 α) under the regulation of prolactin initiates parturition via targeting the myometrium to incite smooth muscle contraction.^{10–12} *Trp53*-deficient decidua fails to support the progress of pregnancy to full-term with 50% incidence of preterm birth due to derailed mTOR signaling pathway and insufficient COX2-derived PGF2 α .¹³ However, the detailed roles of decidua in parturition regulation remain enigmatic.

The maternal-fetal interface is separated to decidua zone and placental zone based on the distribution of the trophoblast giant cells (TGC).¹⁴ The maternal decidua zone is a highly dynamic and heterogenetic region consisting of different decidualized stromal cells, epithelial cells, endothelial cells, perivascular cells, lymphatic cells, and immune cells.^{15,16} Among them, overactivated macrophages or natural killer (NK) cells in the maternal decidua lead to recurrent spontaneous absorption by targeting decidualized stromal cells.^{17,18} Besides, abnormal epithelium-stroma interactions mediated by IHH-PTCH/GLI and HB-EGF-EGFR signaling pathways are also critical for the pathological mechanism of thin endometrium.¹⁹ These evidences established the concept that appropriate endometrial niche supporting different cell types is momentous for decidua homeostasis maintenance, while the landscape of the significance of these cell types remains largely unknown.

In this study, we explore the parturition preparation by investigating the heterogeneity of maternal decidua in mouse while approaching parturition via single-cell RNA sequencing (scRNA-seq), optimized single-cell resolution *in situ* hybridization on tissues (SCRINSHOT), and

¹Fujian Provincial Key Laboratory of Reproductive Health Research, Department of Obstetrics and Gynecology, The First Affiliated Hospital of Xiamen University, School of Medicine, Xiamen University, Xiamen, Fujian 361102, China

²State Key Laboratory of Vaccines for Infectious Diseases, Xiang An Biomedicine Laboratory, School of Medicine, Xiamen University, Xiamen, Fujian, China

³Department of Obstetrics and Gynecology, The Affiliated Hospital of Nantong University, Xisi Road, Nantong, Jiangsu, China

⁴Present address: College of Life Sciences, Wuhan University, Wuhan, China

⁵Present address: Department of Medical Genetics, Center for Medical Genetics, Peking University Health Science Center, Beijing, 100191, China

⁶These authors contributed equally

⁷Lead contact

*Correspondence: haili_bao@163.com (H.B.), haibin.wang@vip.163.com (H.W.), wbdeng@xmu.edu.cn (W.D.)

<https://doi.org/10.1016/j.isci.2023.107796>



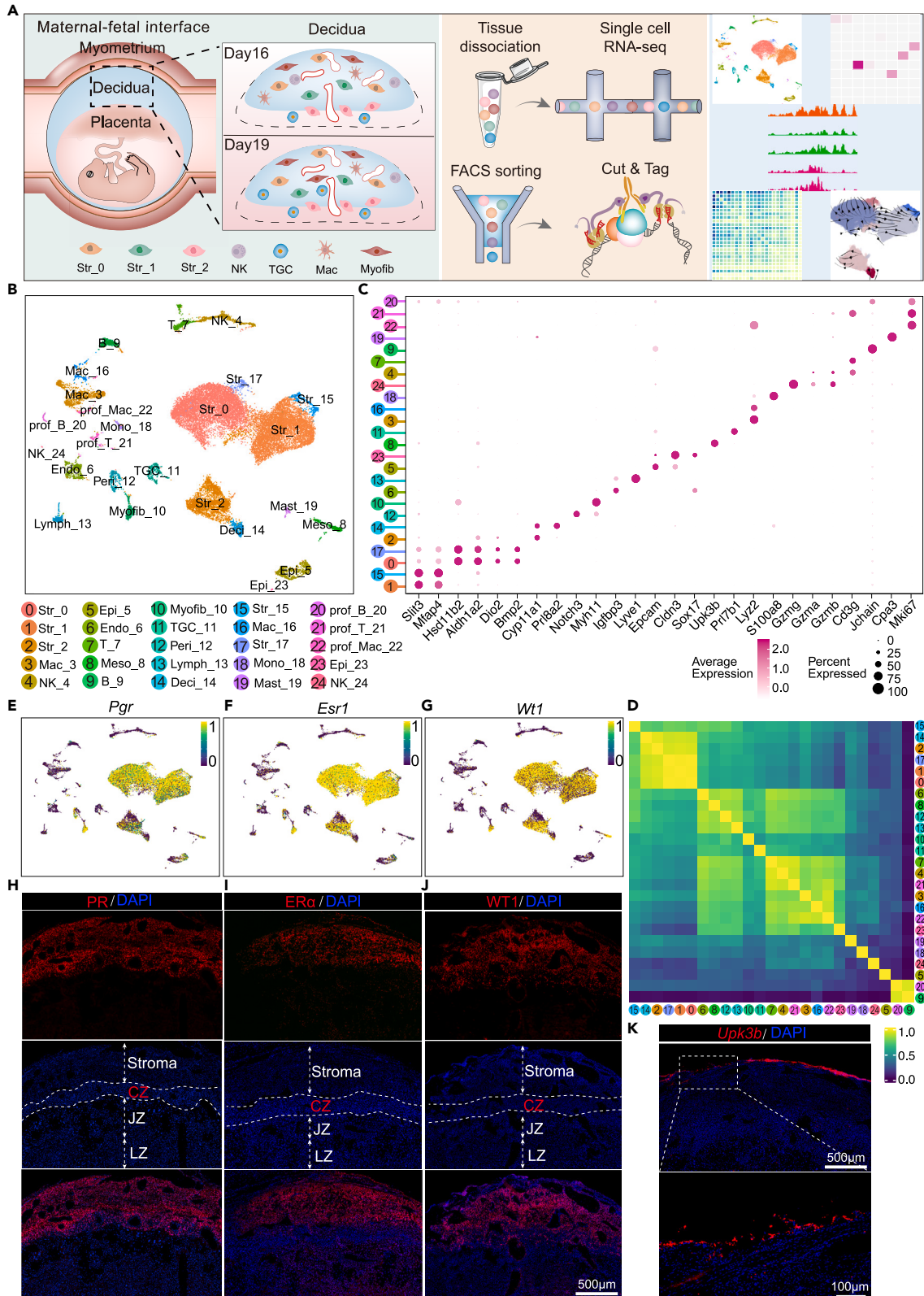


Figure 1. The single-cell landscape of mouse D16 and D19 decidua

(A) Diagram illustrates the experimental workflow for single-cell transcriptome and epigenome profiling in days 16 and 19 decidua. Str_0: stromal cells 0; Str_1: stromal cells 1; Str_2: stromal cells 2; NK: natural killer cells; TGC: trophoblast giant cells; Mac: macrophages; Myofib: myofibroblast cells.
(B) Uniform manifold approximation and projection (UMAP) plot of the major cell types in days 16 and 19 decidua. Dots represent individual cells, and colors represent different cell populations.
(C) The expression of marker genes across different cell types.
(D) The Pearson correlation of genes' expression of different cell types.
(E–G) UMAP visualization of the expression of selected marker genes *Pgr* (D), *Esr1* (F), and *Wt1* (G) in stromal cells.
(H–J) Immunostaining of progesterone receptor (PR) (H), estrogen receptor alpha (ER α) (I), and WT1 transcription factor (WT1) (J) in day 16 decidua. CZ: compacting zone; JZ: junctional zone; LZ: labyrinth zone.
(K) Localization of *Upk3b* mRNA in day 16 decidua.

other molecular measures. Our results unravel that stromal cell is the most abundant and active cell type in decidua and dominates decidual microenvironment by tightly communicating with other cell types. Collectively, this study elucidates a landscape picture for parturition preparation in maternal decidual at single-cell resolution and illustrates the role of stromal cells in calibrating parturition-permission signal in decidua to determine parturition timing.

RESULTS**Cell heterogeneity of maternal decidua by scRNA-seq**

The parturition of mice is initiated at the night of day 19 via labor cascade (day 1 = the day of plug positive) and finished on day 20.²⁰ The maternal deciduae of day 16 (non-labor stage with low expression of contraction-associated proteins: *Oxtr* (Oxytocin receptor) and *Gja1* (Gap junction protein alpha 1)) and day 19 (peri-parturition with higher expression of *Oxtr* and *Gja1*)²¹ were collected in the morning and subjected to scRNA-seq to depict the cell heterogeneity of decidua (Figures 1A, S1A, and S1B). Totally 25 distinct clusters were identified, including five different stromal cells (Str), decidualized stromal cells, endothelial cells, lymphatic endothelial cells, epithelial cells, mesothelium, myofibroblasts, pericytes, TGC, and immune cells (NK cells, macrophages, T cells, neutrophils, B cells, and mast cells) as annotated based on marker genes. Various populations were visualized using uniform manifold approximation and projection (UMAP) (Figures 1B–1D).

Stromal cell was the most abundant cell type as evidenced by the expression of progesterone receptor (PR), estrogen receptor alpha, and WT1 transcription factor (WT1) (Figures 1E–1J). Through the staining of these maternal-specific genes, we noticed that the maternal-fetal interface contained a specific layer with intensive nuclear staining. The co-localization of PR and WT1 with CK8 marked TGC suggested that this nucleus intensive layer containing both maternal and fetal tissue, indicating the invasion of TGC into maternal decidua tissue, termed compact zone hereafter (Figures S2A and S2B).

The presence of endothelial and lymphatic endothelial cells was marked by PECAM1 and LYVE1 separately (Figure S3A). The lymphatic endothelial cells were mainly distributed in maternal myometrium, remodeling vessels, and placenta labyrinth as reported before.^{22,23}

The epithelial cells at implantation site were removed at early pregnancy in mice. At later stage, epithelial cells were gradually repaired from inter-implantation sites and extend to the placenta detach site to facilitate the pups delivery.²⁴ Among those epithelial-specific genes, we surprisingly found that 20 α HSD (*Akr1c18*), the gene responding to progesterone degradation which highly expressed in cervix epithelium but not expressed in uterine epithelium on day 4,²⁵ was highly expressed in day 16 and day 19 epithelium (Figures S3B and S3C). Further study showed that the expression of *Akr1c18* in epithelium emerged as early as day 10 (Figure S3D). Epithelium plays an important role in parturition in both humans and mice. Previous work in mouse cervix suggested that epithelial cell remodeling was necessary to maintain a dynamically shifting state of homeostasis in pregnancy and labor.²⁶ In this study, we also found a special cell type mesothelium located in the utmost outside of the uterus as marked by *Upk3b* (Figure 1K) and *Muc16*. The function of this specific cell type was supposed to reduce the friction and be progenitor of specific cell types.²⁷ Among the populations of immune cells, macrophages were the most abundant cell type which mainly located around myometrium and the underneath of epithelium (Figure S3E). Although NK cells were widely distributed in days 16 and 19 decidua, the proportion of NK cells was significantly decreased in day 19 stroma as measured by FACS and the immunostaining of DBA-lectin, *Gzma*, *Gzmb*, and *Spp1* (Figures S4A–S4H).

Signatures of distinct stromal cells during parturition

As stromal cell was the most abundant cell type in decidua, we first characterized the localization of these different stromal cells utilizing optimized SCRINSHOT.²⁸ Our results suggested that *Hsd11b2* and *Dio2*, which are highly expressed in subepithelial stromal cells on day 4 and rapidly disappeared in differentiated stromal cells after embryo implantation,^{29,30} were specifically expressed in Str_0 stromal cells on day 16. SCRINSHOT showed that *Hsd11b2*-positive Str_0 stromal cells were mainly located in the outer part of decidua and sparsely distributed in whole decidual (Figure 2A). Str_1 stromal cells, marked by *Ptx3*, were widely distributed in whole decidua (Figure 2A). Str_2 stromal cells, marked by *Cyp11a1*, were sparsely distributed in the decidua (Figure 2A).

To depict the functional characterization of these three stromal cells, gene expression clustering was applied in these three stromal cells; genes highly expressed in each stromal cell population were selected and subjected to KEGG analysis (Figures 2B and 2C). Our results unraveled that Str_0 stromal cells marker genes were highly enriched in spliceosome and estrogen signaling pathways. As Str_0 stromal cells were marked by the undifferentiated markers *Dio2* and *Hsd11b2*, the activated spliceosome and estrogen signaling pathway might be involved in the maintenance of this undifferentiated status of stromal cells. It was noteworthy that genes involved with tissue reorganization

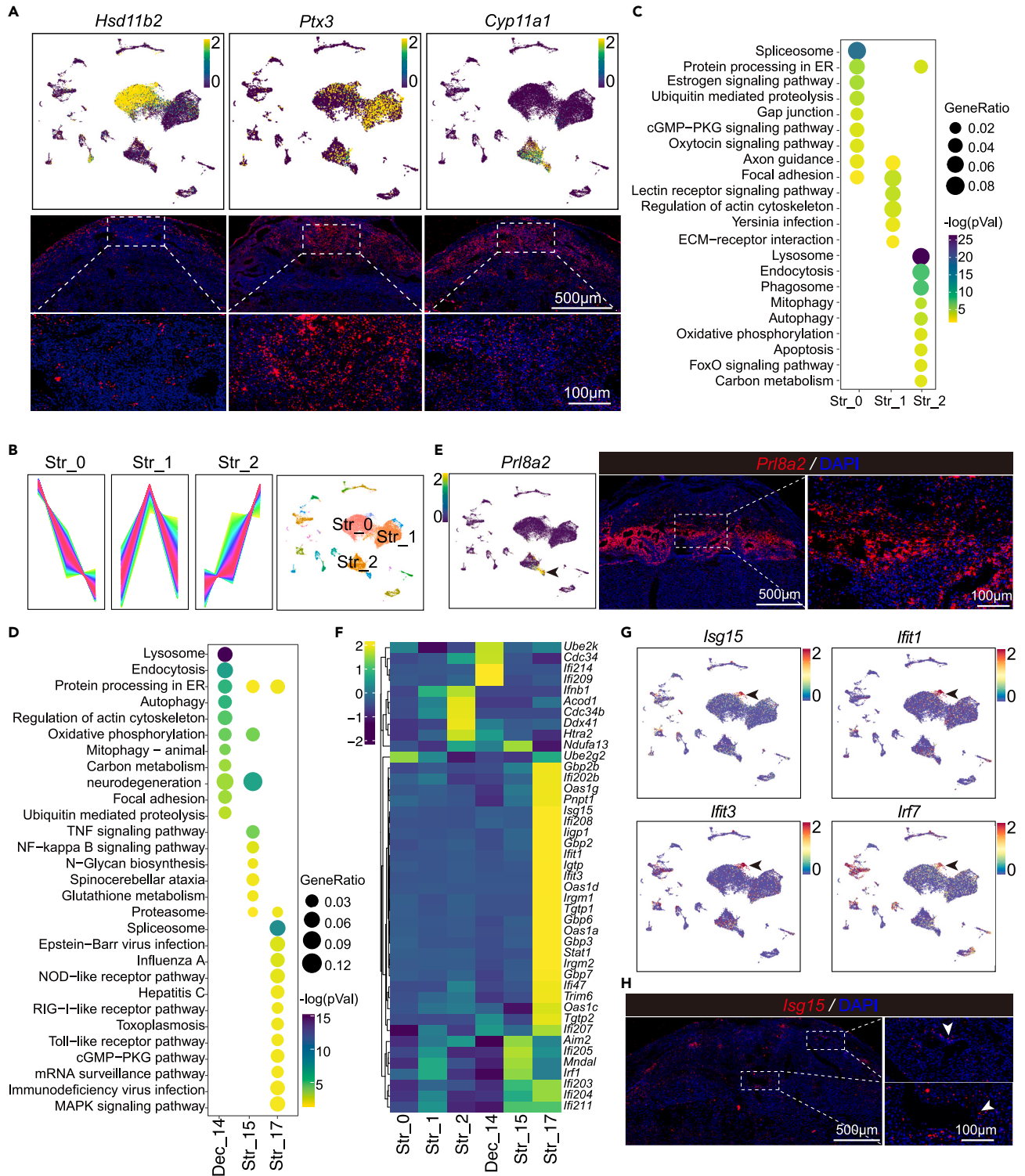


Figure 2. The signature of different stromal cells

(A) The expression and localization of *Hsd11b2*, *Ptx3*, and *Cyp11a1* in Str_0, Str_1, and Str_2, respectively.

(B) Genes highly express in Str_0, Str_1, and Str_2 by gene expression clustering analysis.

(C) The KEGG enrichment of genes highly express in Str_0, Str_1, and Str_2 stromal cells; dot size: number of genes in data attributed to each KEGG term; color bar: the log10 transformation of enrichment p value.

Figure 2. Continued

(D) KEGG enrichment of genes highly express in Dec_14, Str_15, and Str_17 cells; dot size: number of genes in data attributed to each KEGG term; color bar: the log10 transformation of enrichment p value.

(E) The expression and localization of *Prl8a2* mRNA in day 16 decidua. Arrow head indicated the expression of *Prl8a2*.

(F) Heatmap of genes in interferon β (INF β) signaling pathway in different stromal cells and decidualized stromal cells. Colors represent z-scores normalized expression of genes.

(G) The expressions of INF β signaling pathway genes *Isg15*, *Ifit1*, *Ifit3*, and *Irf7* in Str_17. Arrow heads indicate the expression of these genes.

(H) The localization of *Isg15* mRNA in day 16 decidua.

pathways were highly enriched in Str_1 stromal cells, including axon guidance, focal adhesion, and regulation of actin cytoskeleton. This result heralded the obvious structure organization of stromal cells in later stage of pregnancy. The most significantly enriched pathways in Str_2 stromal cells were lysosome, endocytosis, phagosome, and autophagy pathways, which were closely relevant with nutrition supporting and longevity increasing of these stromal cells to adapt with growing embryos.

In addition to these stromal cells, we also noticed some other cell types with smaller populations, such as Dec_14, Str_15, and Str_17. Since Dec_14 stromal cells were close to with Str_2 in UMAP, these cells were also characterized with obvious autophagy pathway as revealed by KEGG analysis (Figure 2D). Additionally, we found that these cells highly expressed decidual marker *Prl8a2* and were mainly localized in the upper part of compact mixture zone (Figure 2E). It was interesting that the expression of HAND2 was also limited in this area (Figures S5A and S5B). Genetic evidence showed that HAND2 is indispensable for embryo implantation and stromal cell decidualization at early stage.³¹ While the expression and function of HAND2 in later stage remains unknown, similar localization of HAND2 with *Prl8a2* suggests that HAND2 would be also important for stromal cells decidualization, which deserves further study in genetically modified animals.

Interferons (IFNs) were proposed to be induced in immune cells as well as cervical epithelial cells in bacterial-induced preterm birth mice based on scRNA-seq.³² In our study, we noticed that infection signaling pathway was overtly enriched in Str_17 (Figure 2D). This observation was further supported by the observation of enriched IFN- β signaling pathway in stromal cells in decidua with specific expression of *Isg15*, *Irf7*, *Ifit1*, and *Ifit3* (Figure 2F), which is further corroborated by the localization of *Isg15* in the perivascular stromal cells (Figures 2G and 2H). Considering the highly phosphorylation of Stat3 under infection insult in our previously study,³³ this result uncovered a cell type against virus infection probably associated with the protection setup of maternal decidua under certain situation.

Stromal cells reorganization during pregnancy

The initiation of parturition was ultimately reflected in muscle contraction. To explore the dynamic change of endometrial smooth muscle, *Myh11*, one of the specific markers of smooth muscle in endometrium, was utilized to chart the localization of smooth muscle. Surprisingly, although there was intensive muscle bundle in the outer of uterus, sparsely distributed smooth muscle was mingled in stromal cells (Figures 3A and 3B). This result was also recapitulated by the staining of *Acta2*, another marker of smooth muscle (Figure 3C). This stromal myometrium distribution in-between might be ascribed to stromal cells invading into myometrium. To decrypt this mystery, we detected the expression of α SMA (*Acta2*) with co-staining with CD31 from days 8 to 16. There was little to no α SMA expression in stromal cells except some α SMA-positive cells surrounding blood vessels in mesometrial pole on days 8 and 10 (Figure 3C), which was supported by previous observation that perivascular cells close to myometrium were marked by both α SMA and NG2 in the outer part of uterus.³⁴ While the smooth muscle distribution in stroma without co-localization with blood vessels was obviously observed from day 12 (Figure 3C). It was feasible to speculate that, accompanied with the deep invasion of TGC into mesometrial pole and the growing of developing embryo, the smooth muscle was tensely stretched and became discontinued with the stromal cells filled in between.

To further explore the potential mechanism of the invasion of these stromal cells into myometrium, we revisited the functional characterization of these stromal cells. We noticed that the axon guidance pathway was significantly enriched in Str_0 and Str_1, including *Slit3*, *Sema3b*, *Robo3*, and *Vegfd* (Figures 3D–3G). *Slit3*-*Robo1* signaling pathway was reported critical for cell migration for neuro and other cell types.^{35–37} Our *in situ* hybridization also revealed that *Slit3* was strongly expressed in stromal cells on day 16 (Figure 3E).

In addition, SEMA3B, a secreted protein that belongs to the class 3 semaphorins, was reported critical for axons guiding;³⁸ our SCRINSHOT results also indicated that *Sema3b* was strongly expressed in stromal cells on day 16 (Figure 3J). SEMA3 members form complexes with two types of cell surface receptors: neuropilins (NRP1 and NRP2) and plexins. Neuropilins provided binding sites for SEMA3 whereas plexins were necessary for signal transduction. In addition to semaphorins, NRP1 and NRP2 also interact with several members of the vascular endothelial growth factor family. Our scRNA-seq and SCRINSHOT results indicated that *Vegfd* was highly expressed in stromal cells while *Nrp2* was specifically expressed in lymphatic endothelial cells and endothelial cells on day 16 (Figures 3H and 3I). The expression of the migration-associated genes in stroma and endothelium indicated the complex communications between these two cell types in guiding mesometrium reorganization (Figure 3K). Summarily, previously described observations suggested that the mesometrial stromal cells and smooth muscles underwent notable reorganization at later stage of pregnancy.

Decidual RA is important for parturition preparation

The maternal tissue needed to be prepared prior to parturition. To depict the dynamic change between day 16 and day 19, we compared cell composition and gene expression in these two different stages. Our results revealed that although the cell composition was comparable between these two different stages, gene expression was significantly altered (Figures 4A–4C). Among them, alcohol dehydrogenase 1 (*Adh1*) was overtly upregulated in almost all stromal cells in day 19 stroma compared with day 16, evidenced by both scRNA-seq and

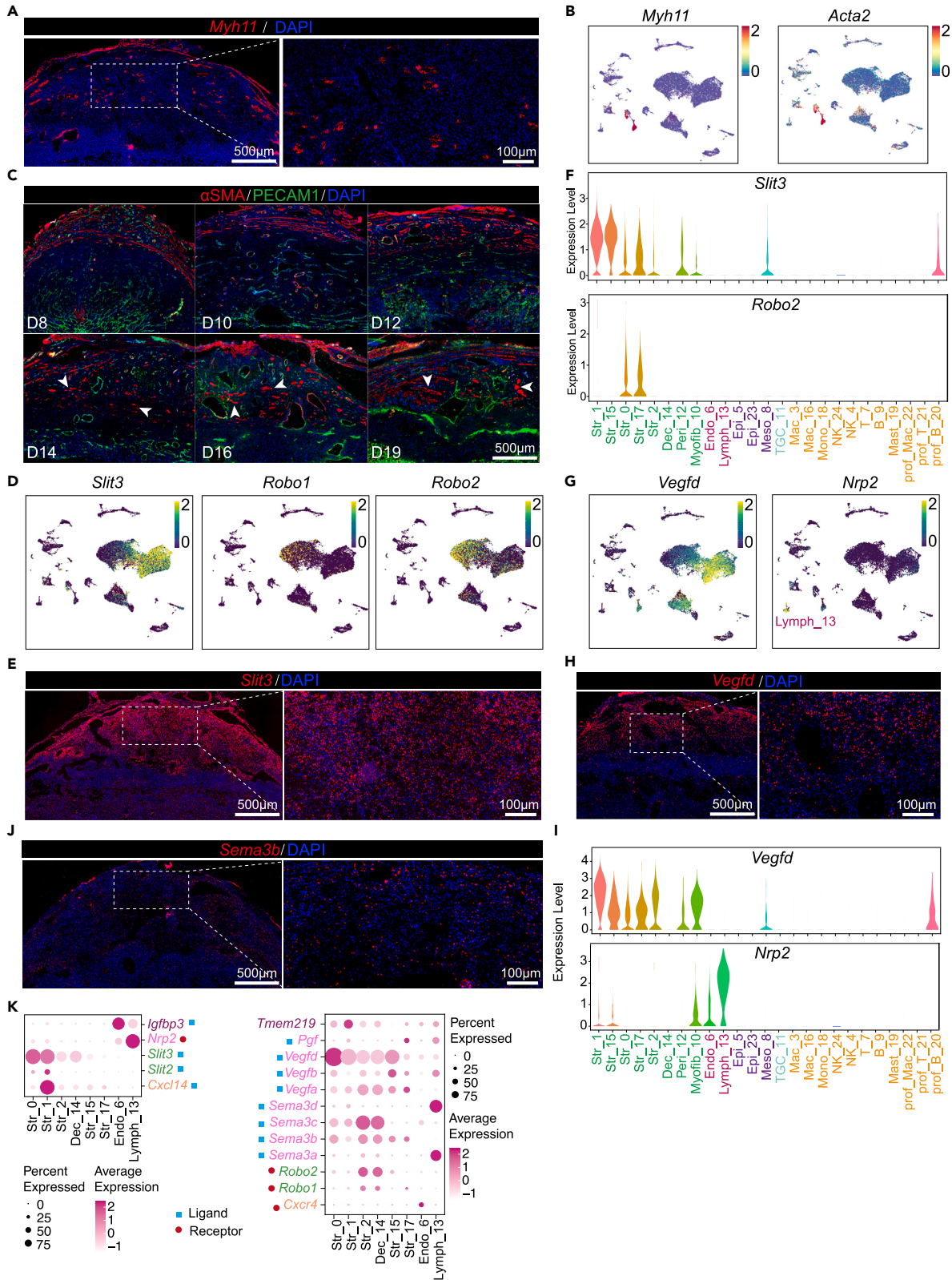


Figure 3. The signaling pathway of stromal cells migration

- (A) The localization of *Myh11* mRNA in day 16 decidua by SCRINSHOT.
(B) The expression of smooth muscle markers *Myh11* and *Acta2* in decidua.
(C) Immunostaining of α SMA (red), PECAM1 (green), and DAPI (blue) in decidua from days 8–19.
(D) The UMAP visualization of the expression of *Slit3* and its receptors *Robo1* and *Robo2* in different cell types.
(E) The localization of *Slit3* mRNA in day 16 decidua.
(F) Violin plots show the expression levels for *Slit3* and *Robo2* in different cell types.
(G) The UMAP visualization of *Vegfd* and its receptor *Nrp2* in different cell types.
(H) The localization of *Vegfd* mRNA in day 16 decidua.
(I) Violin plots show the expression levels for *Vegfd* and *Nrp2* in different cell types.
(J) Localization of *Sema3b* mRNA in day 16 decidua.
(K) The expressions of genes associated with migration signaling pathways. The same color in left and right represent genes in the same signaling pathway with ligands marked with blue and receptors marked with red. The size of the dot represents the percent of cells expressed with indicated genes and the color represents the average expression of indicated gene.

SCRINSHOT (Figures 4D–4F). Additionally, aldehyde dehydrogenase family 1, subfamily A2 (*Aldh1a2*), was also upregulated in day 19 stroma, especially in Str_0 stromal cells (Figures 4G and 4H). As both *Adh1* and *Aldh1a2* were critical enzymes for retinoic acid (RA) metabolism, it was reasonable to suspect that RA plays an important role in parturition preparation. This speculation was further supported by the expression of retinol-binding protein 4 (Figures 4I and S6A) and nuclear receptors of retinoic acid, retinoic acid receptor alpha (*Rara*), retinoic acid receptor gamma (Figure 4J), and retinoid X receptor alpha (*Rxra*). These results indicated that RA synthesis was cumulatively increased approaching parturition. To further interrogate the physiological significance of RA in parturition initiation, all-trans RA (atRA) was injected (800 μ g/mouse/time) from days 16 to 17. Compared with control group, 72.7% mice were parturied before day 19, indicating the role of RA in accelerating the timing of parturition (Figures 4K and 4L). The expressions of these retinoic acid synthesis-related genes were also recapitulated in human maternal stromal cells around parturition,³⁹ further supporting the importance of retinoic acid metabolism in parturition (Figures S7A–S7H).

The next question was the underlying mechanism by which RA induced parturition. We firstly extrapolated the differentially expressed genes between day 16 and day 19. *Oxtr*, the most known gene associated with parturition initiation,⁴⁰ was significantly increased in smooth muscle (Figure S8A). Additionally, our scRNA-seq and SCRINSHOT results also indicated that *Oxtr* expression was increased in Str_0 and Str_1 on day 19 (Figures S8B and S8C), indicating that stroma was another critical parturition initiation site. Connexin 43 (*Gja1*), another critical gene recognized as expressed in smooth muscle approaching parturition in both human and mouse mediating ion and nutrition exchange between cell,⁴¹ was also highly expressed in not only smooth muscle but also stromal cells (Figures S8D–S8F). These expressions of *Oxtr* and *Gja1* in stromal cells were also corroborated with previous studies.^{42,43} Apart from these two genes, matrix metalloproteinase 11 (*Mmp11*), a matrix-degrading enzyme,⁴⁴ was also highly increased in day 19 Str_0 and Str_1 (Figures S8G–S8I). Besides the upregulated genes in day 19 stromal cells, we noticed that the expressions of collagen type I alpha 1 chain (*Col1a1*), proenkephalin (*Penk*), and elastin (*Eln*) were significantly downregulated (Figures 5A–5C), which also supported the concept that parturition was accompanied with dramatic extracellular matrix remodeling to facilitate parturition initiation as well as endometrial postpartum repairing.

To investigate whether RA participated in parturition via regulation of previously mentioned genes, stromal cells from day 16 were isolated and treated by atRA. The results suggested that *Gja1*, *Oxtr*, and *Mmp11* were not affected by RA (Figures S6B–S6D). But the extracellular matrix genes were overtly downregulated by atRA, such as *Col1a1*, *Penk*, *Eln*, fibronectin (*Fn1*), and *Postn* (Figure 5D) and others (Figures S6E and S6F). As 10X genomics scRNA-seq only detected the genes at 3' UTR, to thoroughly enumerate the genes' dynamic changes in day 16 and 19 stroma, sorted stromal cells were subjected to high-throughput bulk RNA sequencing. The results also confirmed that those extracellular-related genes were significantly downregulated (Figures 5E–5H).

As the change of gene expression was accompanied with epigenetic modification, to chart the epigenetic landscape of stromal cells approaching parturition, CUT&Tag was applied to inspect epigenetic changes in purified stromal cells from both days 16 and 19 (Figure S9A). The distribution curve and heatmap of H3K4me3, H3K4me1, and H3K27Ac confirmed the high quality of our CUT&Tag data (Figures 5I and 5J). To detailed segmentation of genome regions modified by these epigenetic modification combinations, ChromHMM was applied to figure out the modification pattern of genome by these enzymes. There were totally eight modification patterns with pattern 6 possessed high enrichment of H3K4me3, H3K4me1, and H3K27Ac with low H3K27me3 (Figure 5K). Although the total modifications of H3K27Ac and H3K4me1 were comparable genome widely in days 16 and 19 (Figure 5L), the alternations in specific sites were observed. For *Oxtr* and *Mmp11*, both H3K4me1 and H3K27Ac at the marked site were responded for their upregulation in day 19. H3K27Ac at the marked site was more dominant for *Aldh1a2* and *Adh1* expression (Figure 5M). Interestingly, both the marked sites responded for these gene expression well correlated with pattern 6 characterized by ChromHMM. These results suggested that the epigenetic landscape of stromal cells was also involved in parturition preparation.

The cell connections in days 16 and 19 decidua

Cell-cell communications play an important role in homeostasis maintenance. In order to dissect out the complex interactions between different cell types, we next leveraged CellPhoneDB to identify the expression of ligand-receptor pairs and to predict their interactions with other cells in days 16 and 19 decidua. As ranked by the number of connections between different cell types, Str_15, Str_1, Str_17, Str_0, and endothelial cell were the most active cell types in days 16 and 19 decidua (Figures 6A, 6B, and S10A). Besides, both

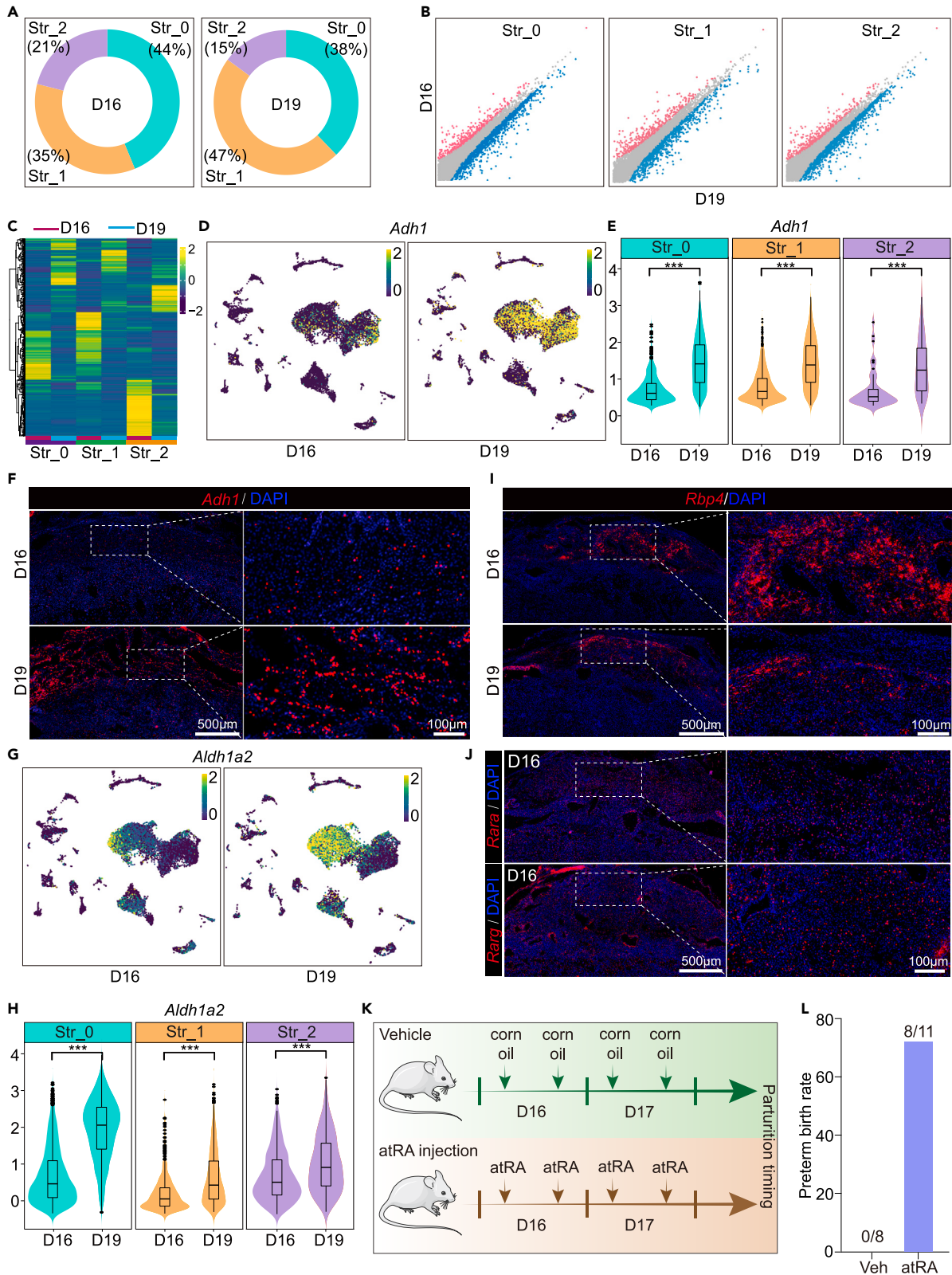


Figure 4. Decidual retinoic acid synthesis during parturition preparation

- (A) Stromal cell composition in days 16 (left circle) and 19 (right circle) decidua.
- (B) Scatterplots depict differentially expressed genes in Str_0, Str_1, and Str_2 between day 16 and day 19. Red and blue represent genes specifically expressed in day 16 and day 19, respectively.
- (C) Heatmap of the differentially expressed genes in Str_0, Str_1, and Str_2 between day 16 and day 19. Color bar represents Z score normalized expression of genes.
- (D) UMAP visualization of the expression of *Adh1* in days 16 and 19 stromal cells in decidua.
- (E) Quantitative expression of *Adh1* in distinct stromal cells between days 16 and 19. *** $p < 0.001$, Wilcoxon tests.
- (F) Localization of *Adh1* mRNA in days 16 and 19 decidua.
- (G) UMAP visualization of the expression of *Aldh1a2* in days 16 and 19 stromal cells in decidua.
- (H) Quantitative expression of *Aldh1a2* in distinct stromal cells between days 16 and 19. *** $p < 0.001$, Wilcoxon tests.
- (I) Localization of *Rbp4* mRNA in days 16 and 19 decidua.
- (J) Localization of *Rara* and *Rarg* mRNAs in days 16 and 19 decidua.
- (K) Experimental schedule of atRA administration induced preterm birth in D16-D17 pregnant female mice (i.p. injection with 800 $\mu\text{g}/\text{mouse}$ each time).
- (L) The ratio of preterm birth after atRA injection.

CellPhoneDB and NicheNet analysis strongly suggested that there were extensive communications between endothelial cells and stromal cells (Figures 6C and S10B). Especially, endothelin 1 (*Edn1*) in endothelial cells was of high priority to regulate downstream target genes expression through its receptor *Ednra* and *Ednrb* (Figure 6D). EDN1 was reported to activate RhoA/Rho kinase pathway through protein kinase C and sphingosine kinase to promote the calcium sensitization and subsequent contraction of rat myometrium in the late pregnancy.^{45,46} Our results suggested that there was less EDN1 secreted by vascular endothelial cells in day 16 decidua with more in epithelium, while in day 19 decidua, stronger vascular endothelial EDN1 was secreted to target stroma and other cell types (Figures S11A–S11G).

Among the differentially changed pathways, P-selectin (SELP)-CD34 signal pathway increased obviously in day 19 stroma with FN1-integrin-mediated extracellular matrix organization and bone morphogenetic protein-mediated differentiation pathways downregulation as evidenced by both scRNA-seq and SCRINSHOT (Figures 6E, S11H, and S11I). The SELP gene encoded a cell adhesion molecule facilitating the interaction of activated platelets on endothelium with leukocytes,⁴⁷ which supported the conjecture of postpartum coagulation and wound healing. In summary, our explorations of the signaling pathway between stroma and other types of cells confirmed the complex interactions of different cell types involved for parturition preparation.

The stemness genes were activated before parturition

To delineate the functional change of differentially expressed genes between days 16 and 19, the enriched pathways in different stromal cells were analyzed. It was noticeable that regulation of pluripotency and WNT signaling pathway were enriched in day 19 stroma, including *Wnt5a*, *Axin2*, *Fzd7*, *Dkk2*, and *Ror2* (Figures 7A–7F). When projecting these signaling pathways to the cells, it showed that WNT signaling was mainly enriched in Str_0 and Str_1 and regulation of pluripotency was enriched in Str_0 (Figures 7G and 7H). AXIN2-mediated WNT signaling pathway was reported as critical gene for progenitor cells regeneration.⁴⁸ The RNA velocity analysis also confirmed that Str_0 stromal cells were potential progenitors of Str_1 (Figure 7I).

DISCUSSION

Parturition is regulated by progressive cascade of events, comprising signaling pathways from both maternal decidua and placenta, while the underlying mechanism has been a long-standing conundrum. Previous studies suggest that the development of placenta controls the timing of parturition through “placenta clock.”⁴⁹ Accumulative evidence shows that decidua plays an essential role during parturition via “decidua clock.”⁵⁰ Both genetic and epigenetic predisposition of decidua and external inflammation insults are considered the most important determinants for the irregular parturition initiation.⁵¹ Current understanding for the parturition initiation is that PGF2 α derived from maternal decidua or fetal membrane induces luteolysis and smooth muscle contraction.^{3,12} This work has been further proven by the observation of delayed parturition in COX-1-deficient mice.⁵² The failure of labor onset is observed in PGF2 α receptor (FP) knockout mice accompanied with defect *Oxtr* induction but normal *Oxtr* expression.⁵³ However, it is interesting that *Oxtr* is dispensable for parturition onset since *Oxtr* deficiency exhibits normal parturition but with defects in lactation and maternal nurturing.⁵³ Whether there are some other decidual factors required for induction of parturition remain elusive.

Among decidual stromal cells, in this study, we depict the decidua factors by single-cell sequencing. Stromal cell is the most abundant cell type in maternal decidua. The scRNA-seq data of the early maternal-fetal interface in human show that there were three clusters of stromal cells in decidual layers.¹⁶ Decidual stromal cells play critical roles in promoting successful pregnancy, interfacing with fetal cells throughout pregnancy, and the timing of birth.^{3,54} Both genetic and epigenetic predisposition of decidual stromal cells are considered the most important determinants for the irregular parturition initiation. The expression of GATA2 and HAND2 in stromal cells may regulate transcriptional programs that influence the timing of parturition in humans.⁵¹ Our study suggests that the composition of decidua is more complex than we knew before. There are five different stromal cells and one decidualized stromal cell in decidua with their own roles in mice at later stage of pregnancy. The complexity of stromal cell in decidua approaching parturition is further corroborated by another work investigating the underlying mechanism of bacteria-induced preterm birth.³² In our study, we further characterize the regionalization of different stromal cells in decidua as well as decidualized stromal cells.

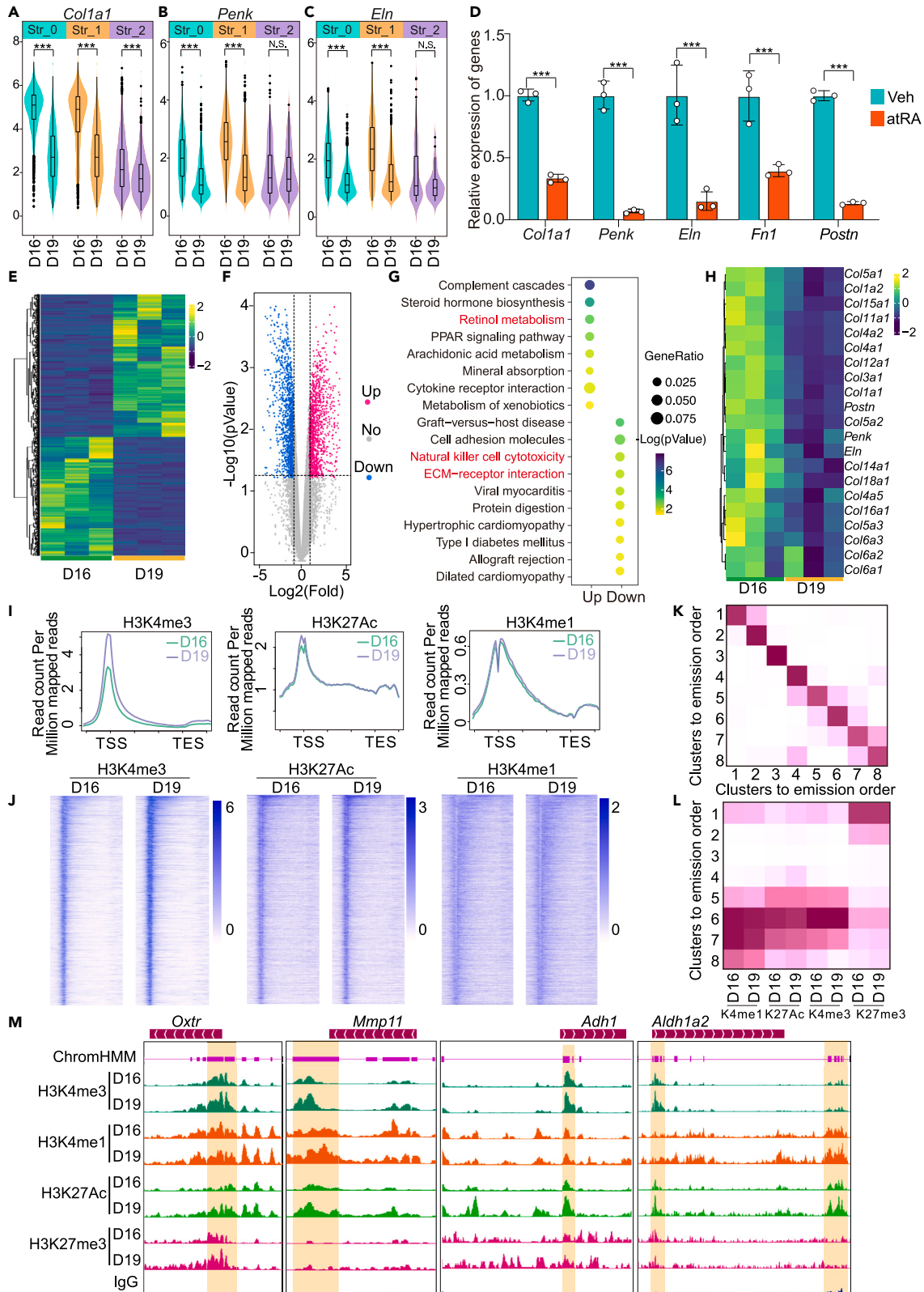


Figure 5. The downstream genes of RA and the epigenetic landscape of stromal cells approaching parturition

- (A–C) Quantitative expression of *Col1a1* (A), *Penk* (B), and *Eln* (C) in distinct stromal cells between days 16 and 19. ***p < 0.001, Wilcoxon tests.
- (D) Relative expression of *Col1a1*, *Penk*, *Eln*, *Fn1*, and *Postn* mRNAs in day 16 cultured stromal cell after 5 μ M atRA treatment for 24 h. ***p < 0.001, Student's t test. Data are represented as mean \pm SEM (n = 3).
- (E) Heatmap of differentially expressed genes by bulk RNA-seq in whole decidua from days 16 and D19; Colors represent the Z score normalized expression of genes.
- (F) Volcano plot of differentially expressed genes by bulk RNA-seq in whole decidua between days 16 and 19. Red color represents of upregulated genes in day 19 decidua with p < 0.05 and fold change >2; blue color represents downregulated genes in day 19 decidua with p < 0.05 and fold change <0.5; gray color represents not significantly change genes in these two groups.
- (G) Dot plot of enriched signaling pathways based on differentially expressed genes by bulk RNA-seq between day 16 and day 19 decidua.
- (H) Heatmap of extracellular matrix genes in days 16 and 19 decidua by bulk RNA-seq.
- (I) Metaplot of H3K4me3, H3K27Ac, and H3K4me1 modification across gene body. TSS, transcription start site; TES, transcription end site.
- (J) Heatmap of H3K4me3, H3K27Ac, and H3K4me1 distribution across gene body in days 16 and 19 stromal cells.
- (K) Chromatin state adjacency frequencies (how often 2 chromatin states neighbor each other) defined by multivariate hidden Markov model-based method (ChromHMM) via integrating chromatin modification of H3K4me1, H3K4me3, H3K27Ac, and H3K27me3. Genome is segmented into 200-bp intervals based on state classifications and divided into 8 different modification signatures.
- (L) Definition of distinctive genomic regions marked by H3K4me1, H3K4me3, H3K27Ac, and H3K27me3 which learned by ChromHMM based on the CUT&Tag data.
- (M) The visualizations of H3K4me3, H3K4me1, H3K27Ac, and H3K27me3 modification at *Oxtr*, *Mmp11*, *Adh1*, and *Aldh1a2* loci in IGV. The magenta track represents pattern six defined by ChromHMM in (L) with higher modification of H3K4me1, H3K27Ac, and H3K4me3 and weaker modification of H3K27me3. The red boxes highlight the regions with differential modifications in one of H3K4me3, H3K4me1, and H3K27Ac.

Especially, the stromal cells possess the property of generating local retinol acid characterized by expression of the enzymes for RA syntheses and transports as well as its nuclear receptors, RARa, RARb, and RXRa. The expression of these genes in peri-implantation uterus and compromised female fertility of disrupted RARa also supports the role of RA in pregnancy.^{55,56} Current metabolome profile analysis in maternal plasma evidence that the metabolism during pregnancy is a dynamic and precisely programmed process.⁵⁷ Since adequate vitamin A during pregnancy is of critical importance for the health of pregnant women,⁵⁸ the analysis of retinoid metabolites in pregnant women plasma shows that retinol levels are significantly reduced with significantly increased 13-cis-retinoic acid and retinol-binding protein in PTB compared to term birth.⁵⁹ These metabolic observations further corroborate our conclusion that RA is a potential decidual critical factor for labor onset. More elegant genetic models are deserved to parse the physiological significance of these genes' role during parturition.

The decidua needs to be prepared before parturition including the remodeling of stromal cells which involves the previous unappreciated migration of stromal cells into myometrium in normal physiological condition. Our results suggest that there is dramatic stromal reorganization during pregnancy. During this process, we decipher the mechanism that SLIT-ROBOs signaling pathway is important for this stromal migration. This transformation would benefit the prevention of over-invasion of trophoblast, which would contribute to placenta accreta or placenta implantation in human beings.⁶⁰ This process might also facilitate the muscle contraction in parturition establishment. In addition, the invasion of stromal cells into myometrium would also preserve stromal cells for endometrium regeneration after parturition via WNT signaling pathway.

Tissues destruction, repairing, and remodeling is critical for parturition, placenta shedding, and uterine involution,⁶¹ while little is known about this process until now. Our results suggest that stromal cells play a vital role for the detachment of fetus from uterus via the degradation of extracellular matrix, encompassing kinds of collagens, fibronectin, glycoprotein, and others.^{62,63} Extracellular matrix degradation and remodeling by proteolytic enzymes, such as matrix metalloproteinases (MMPs), are required for the final steps of parturition via their proteolytic activities on specific substrates: collagenases (MMP1,8, and 13), gelatinases (MMP2 and 9), matrilysins (MMP7 and 26), stromelysins (MMP3, 10, and 11), and membrane-type MMPs (MMP14, 15, 16, 17, 24, and 25), and are balanced by the action of their inhibitors.^{64,65}

Our results not only identify the unappreciated role of stromal MMP11, also named as stromelysin-3, holding strong activity to degrade serine protease inhibitor α 1-antitrypsin and insulin-like growth factor-binding protein-1,⁶⁶ in stroma approaching parturition, but also provide evidence that increased RA is important for collagen degradation by inhibiting the expression of sorts of collagenases. Additionally, there are evidences that MMP11 is also important for migration and invasion which corroborates the fact of invasion of stromal cells into myometrium.⁶⁷ Our observations provide a possibility to intervene parturition by targeting extracellular matrix remodeling. Considering the secretory nature of MMP11, it is very promising to predict parturition timing and diagnose preterm birth by monitoring serum level of MMP11.

The recognition of preparation and onset of the labor is very limited until now. PTB, a symptom of derailed initiation of parturition, is increasingly recognized as an outcome that results from a variety of pathological processes. Our results provide information on the parturition preparation and labor onset based on the observation of distinct function of various stromal cells in decidua. In addition, we also unravel that RA is another critical factor for parturition preparation partly by regulating extracellular matrix remodeling (Figure 7J). Collectively, our results shed light on the mechanism of parturition and provide agenda to illuminate the basic and translational research opportunities and limitations that need to be decrepted to advance the field of PTB prevention.

Limitations of the study

Although our research provides a molecular mechanism for the regulation of initiation of labor and PTB, this study has several limitations due to the complexity of regulation mechanisms of delivery initiation and PTB. Firstly, the decidua is a highly heterogeneous tissue consisting of

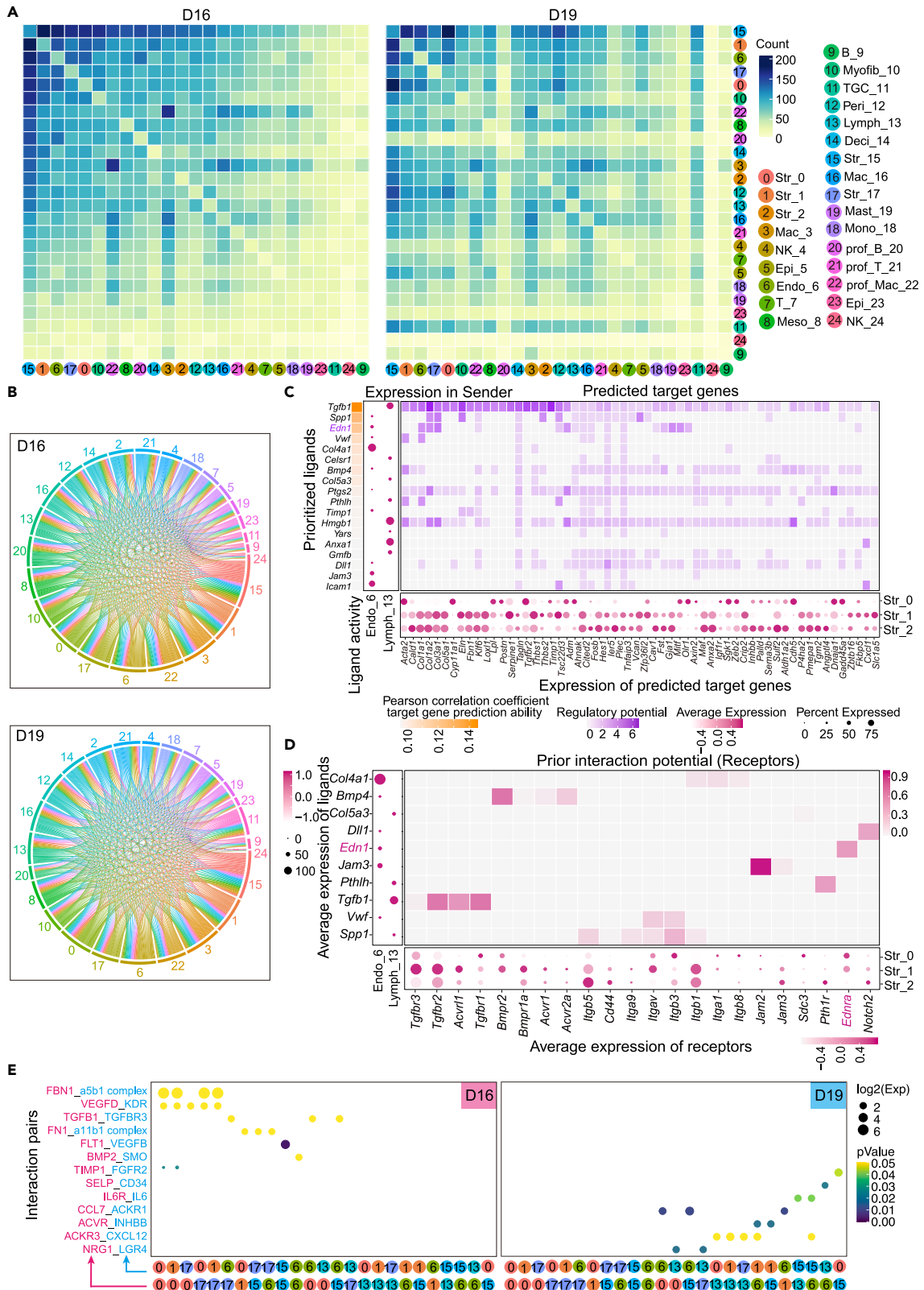


Figure 6. Cell-to-cell connection in day 16 and day 19 decidua

(A) The abundance of connection between different cell types in days 16 and 19 decidua utilizing CellPhoneDB.
(B) The circular plot represents outgoing signaling and incoming signaling among different cell types in days 16 and 19 decidua analyzed by CellPhoneDB.
(C) The interaction between endothelium and lymphatic endothelial cells with the major stromal cells. The most left is the prioritized ligands defined by NicheNet. Pearson correlation indicates the ability of each ligand to its target genes, and better predictive ligands are thus ranked higher. The dot plots represent the expression of ligands in endothelium and lymphatic endothelial cells and their target genes in different stromal cells. Heatmap shows the predicted ligands activity by NicheNet on their target genes in different stromal cells.
(D) Heatmap shows the bona fide interactions between the ligands in endothelium and lymphatic endothelial cells and their receptors in different stromal cells. Dot plots represent the average expression of ligands and their receptors in senders and receivers, respectively.
(E) The differential changed signaling pathways between endothelium, lymphatic endothelial cells, and different stromal cells in day 16 and day 19 defined by CellPhoneDB. Among them, BMP2-SMO and VEGFD-KDR are mainly enriched in day 16 decidua, while SELP-CD34 and ACVR-INHBB are mainly enriched in day 19. The size of dot represents the expression of indicated ligand (magenta) and its receptor (blue) in different cell types and color bar represents their enrich significance. The numbers in the colored round indicate different cell types as annotated in (A).

stromal cells, immune cells, endothelial cells, and other cell types. The expression of various molecules is not only cell type specific but also spatiotemporal specific. To further explore the mechanism of parturition initiation, spatial transcriptome sequencing can be used to conduct in-depth research. Secondly, although our study find that RA plays an important role in the initiation of parturition, more elegant genetic models are deserved to parse the physiological significance of RA during parturition. Thirdly, whether the effect of RA is conservative in clinical practice needs further verification.

STAR★METHODS

Detailed methods are provided in the online version of this paper and include the following:

- KEY RESOURCES TABLE
- RESOURCE AVAILABILITY
 - Lead contact
 - Material availability
 - Data and code availability
- EXPERIMENTAL MODEL AND SUBJECT DETAILS
 - Animals
- METHOD DETAILS
 - 10x genomics single-cell RNA-seq of decidua tissue
 - Flow cytometry staining and cell sorting
 - Decidua stromal cell culture
 - CUT&Tag assay
 - Bulk RNA-Seq of decidual stromal cells
 - RNA-seq data analysis
 - Digoxigenin *In situ* hybridization (ISH)
 - Single-molecule fluorescence *in situ* hybridization (ISS)
 - Immunofluorescence
 - Quantitative real-time PCR
 - Single cell RNA-seq data processing
 - Cell clustering and annotation
 - Gene-clustering analysis
 - Calculation of gene signature scores based on scRNA-seq data
 - Cell-cell interactions analysis by CellPhoneDB
 - CellChat analysis of cell-cell communication
 - RNA velocity analysis
 - Statistical analysis

SUPPLEMENTAL INFORMATION

Supplemental information can be found online at <https://doi.org/10.1016/j.isci.2023.107796>.

ACKNOWLEDGMENTS

This work was supported by the National Key R&D Program of China (2022YFC2704500 and 2022YFC2704600 to W.D.; 2021YFC2700302 to H.W.; 2022YFC2702400 to J.L.), Basic Science Center Program of the National Natural Science Foundation of China (82288102 to H.W.), and National Natural Science Foundation of China (82122026, 32171117, and 81971419 to W.D.; 81830045 and 82030040 to H.W.; 8222026 and 32270907 to S.K.; 31971071 to J.L.).

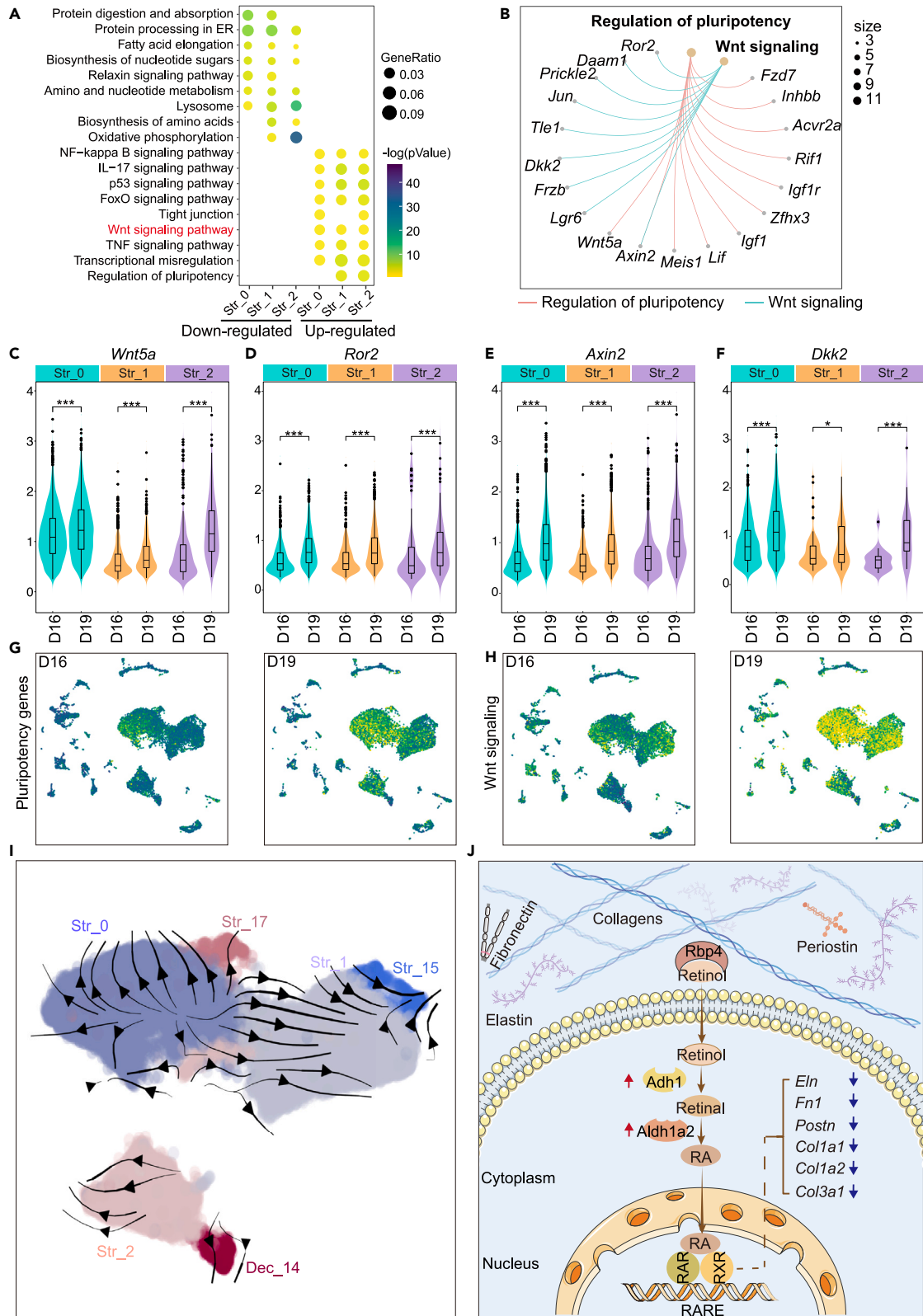


Figure 7. The activity of WNT signaling pathway in stromal cells between day 16 and day 19

- (A) The functional enrichment analysis of differentially expressed genes among three stromal cells between day 16 and day 19 by scRNA-seq.
(B) The networks of pluripotency and WNT signaling pathway-related genes.
(C–F) Quantitative expression of *Wnt5a* (C), *Ror2* (D), *Axin2* (E), and *Dkk2* (F) in distinct stromal cells between days 16 and 19. *** $p < 0.001$, Wilcoxon tests.
(G) Expression of pluripotency signature genes in day 16 and day 19 decidua.
(H) Expression of WNT signaling pathway signature genes in day 16 and day 19 decidua.
(I) The RNA velocity map of different stromal cells.
(J) Summary diagram of the retinoid pathway in parturition. Retinol is transferred into stromal cells by RBP4 and metabolized to retinal by retinol dehydrogenases ADH1. Retinal is further converted to retinoic acid (RA) by ALDH1A2. After binding with its nuclear receptors RARs and RXRs (heterodimers or homodimers), RA affects the expression of sort of extracellular matrix-associated genes. RBP4, retinol-binding protein 4; RAR, retinoic acid receptor; RARE, retinoic acid response element; RXR, retinoid X receptor; RA, retinoic acid.

AUTHOR CONTRIBUTIONS

H.Z., Y.W., H.X., M.L., S.Z., Z.L., H.C., Y.W., and X.X. performed experiments and prepared figures. W.D., H.W., H.B., X.Y., S.K., and J.L. designed experiments. W.D. and H.Z. analyzed data. W.D., H.Z., H.B., and H.W. wrote the manuscript.

DECLARATION OF INTERESTS

The authors declare no competing interests.

Received: March 13, 2023

Revised: May 23, 2023

Accepted: August 29, 2023

Published: September 1, 2023

REFERENCES

1. Goldenberg, R.L., Culhane, J.F., Iams, J.D., and Romero, R. (2008). Epidemiology and causes of preterm birth. *Lancet* 371, 75–84. [https://doi.org/10.1016/S0140-6736\(08\)60074-4](https://doi.org/10.1016/S0140-6736(08)60074-4).
2. Muglia, L.J., and Katz, M. (2010). The enigma of spontaneous preterm birth. *N. Engl. J. Med.* 362, 529–535. <https://doi.org/10.1056/NEJMra0904308>.
3. Norwitz, E.R., Bonney, E.A., Snegovskikh, V.V., Williams, M.A., Phillippe, M., Park, J.S., and Abrahams, V.M. (2015). Molecular Regulation of Parturition: The Role of the Decidual Clock. *Cold Spring Harb. Perspect. Med.* 5, a023143. <https://doi.org/10.1101/cshperspect.a023143>.
4. Moster, D., Lie, R.T., and Markestad, T. (2008). Long-term medical and social consequences of preterm birth. *N. Engl. J. Med.* 359, 262–273. <https://doi.org/10.1056/NEJMoa0706475>.
5. Cappelletti, M., Doll, J.R., Stankiewicz, T.E., Lawson, M.J., Sauer, V., Wen, B., Kalinichenko, V.V., Sun, X., Tilburgs, T., and Divanovic, S. (2020). Maternal regulation of inflammatory cues is required for induction of preterm birth. *JCI Insight* 5, e138812. <https://doi.org/10.1172/jci.insight.138812>.
6. Cha, J., Sun, X., and Dey, S.K. (2012). Mechanisms of implantation: strategies for successful pregnancy. *Nat. Med.* 18, 1754–1767. <https://doi.org/10.1038/nm.3012nm.3012>.
7. Motomura, K., Romero, R., Galaz, J., Tao, L., Garcia-Flores, V., Xu, Y., Done, B., Arenas-Hernandez, M., Miller, D., Gutierrez-Contreras, P., et al. (2022). Fetal and maternal NLRP3 signaling is required for preterm labor and birth. *JCI Insight* 7, e158238. <https://doi.org/10.1172/jci.insight.158238>.
8. Murray, S.A., Morgan, J.L., Kane, C., Sharma, Y., Heffner, C.S., Lake, J., and Donahue, L.R. (2010). Mouse gestation length is genetically determined. *PLoS One* 5, e12418. <https://doi.org/10.1371/journal.pone.0012418>.
9. Nancy, P., Tagliani, E., Tay, C.S., Asp, P., Levy, D.E., and Erlebacher, A. (2012). Chemokine gene silencing in decidual stromal cells limits T cell access to the maternal-fetal interface. *Science (New York, N.Y.)* 336, 1317–1321. <https://doi.org/10.1126/science.1220030>.
10. Challis, J.R.G., Sloboda, D.M., Alfaidy, N., Lye, S.J., Gibb, W., Patel, F.A., Whittle, W.L., and Newnham, J.P. (2002). Prostaglandins and mechanisms of preterm birth. *Reproduction (Cambridge, England)* 124, 1–17. <https://doi.org/10.1530/rep.0.1240001>.
11. Hirota, Y., Daikoku, T., Tranguch, S., Xie, H., Bradshaw, H.B., and Dey, S.K. (2010). Uterine-specific p53 deficiency confers premature uterine senescence and promotes preterm birth in mice. *J. Clin. Invest.* 120, 803–815. <https://doi.org/10.1172/JCI40051>.
12. Li, W.J., Lu, J.W., Zhang, C.Y., Wang, W.S., Ying, H., Myatt, L., and Sun, K. (2021). PGE2 vs PGF2alpha in human parturition. *Placenta* 104, 208–219. <https://doi.org/10.1016/j.placenta.2020.12.012>.
13. Hirota, Y., Cha, J., Yoshie, M., Daikoku, T., and Dey, S.K. (2011). Heightened uterine mammalian target of rapamycin complex 1 (mTORC1) signaling provokes preterm birth in mice. *Proc. Natl. Acad. Sci. USA* 108, 18073–18078. <https://doi.org/10.1073/pnas.1108180108>.
14. Simmons, D.G., Fortier, A.L., and Cross, J.C. (2007). Diverse subtypes and developmental origins of trophoblast giant cells in the mouse placenta. *Dev. Biol.* 304, 567–578. <https://doi.org/10.1016/j.ydbio.2007.01.009>.
15. Suryawanshi, H., Morozov, P., Straus, A., Sahasrabudhe, N., Max, K.E.A., Garzia, A., Kustagi, M., Tuschl, T., and Williams, Z. (2018). A single-cell survey of the human first-trimester placenta and decidua. *Sci. Adv.* 4, eaau4788. <https://doi.org/10.1126/sciadv.aau4788>.
16. Vento-Tormo, R., Efremova, M., Botting, R.A., Turco, M.Y., Vento-Tormo, M., Meyer, K.B., Park, J.-E., Stephenson, E., Polanski, K., Goncalves, A., et al. (2018). Single-cell reconstruction of the early maternal-fetal interface in humans. *Nature* 563, 347–353. <https://doi.org/10.1038/s41586-018-0698-6>.
17. Aikawa, S., Deng, W., Liang, X., Yuan, J., Bartos, A., Sun, X., and Dey, S.K. (2020). Uterine deficiency of high-mobility group box-1 (HMGB1) protein causes implantation defects and adverse pregnancy outcomes. *Cell Death Differ.* 27, 1489–1504. <https://doi.org/10.1038/s41418-019-0429-z>.
18. Du, L., Deng, W., Zeng, S., Xu, P., Huang, L., Liang, Y., Wang, Y., Xu, H., Tang, J., Bi, S., et al. (2021). Single-cell transcriptome analysis reveals defective decidua stromal niche attributes to recurrent spontaneous abortion. *Cell Prolif.* 54, e13125. <https://doi.org/10.1111/cpr.13125>.
19. Lv, H., Zhao, G., Jiang, P., Wang, H., Wang, Z., Yao, S., Zhou, Z., Wang, L., Liu, D., Deng, W., et al. (2022). Deciphering the endometrial niche of human thin endometrium at single-cell resolution. *Proc. Natl. Acad. Sci. USA* 119, e2115912119. <https://doi.org/10.1073/pnas.2115912119>.
20. McCarthy, R., Martin-Fairey, C., Sojka, D.K., Herzog, E.D., Jungheim, E.S., Stout, M.J., Fay, J.C., Mahendroo, M., Reese, J., Herington, J.L., et al. (2018). Mouse models of preterm birth: suggested assessment and reporting guidelines. *Biol. Reprod.* 99, 922–937. <https://doi.org/10.1093/biolre/iy109>.
21. Shchuka, V.M., Abatti, L.E., Hou, H., Khader, N., Dorogin, A., Wilson, M.D., Shynlova, O., and Mitchell, J.A. (2020). The pregnant myometrium is epigenetically activated at contractility-driving gene loci prior to the

- onset of labor in mice. *PLoS Biol.* 18, e3000710. <https://doi.org/10.1371/journal.pbio.3000710>.
22. Collins, M.K., Tay, C.S., and Erlebacher, A. (2009). Dendritic cell entrapment within the pregnant uterus inhibits immune surveillance of the maternal/fetal interface in mice. *J. Clin. Invest.* 119, 2062–2073. <https://doi.org/10.1172/JCI38714>.
 23. Pawlak, J.B., Bálint, L., Lim, L., Ma, W., Davis, R.B., Benyó, Z., Soares, M.J., Oliver, G., Kahn, M.L., Jakus, Z., and Caron, K.M. (2019). Lymphatic mimicry in maternal endothelial cells promotes placental spiral artery remodeling. *J. Clin. Invest.* 129, 4912–4921. <https://doi.org/10.1172/JCI120446>.
 24. Welsh, A.O., and Enders, A.C. (1983). Occlusion and reformation of the rat uterine lumen during pregnancy. *Am. J. Anat.* 167, 463–477. <https://doi.org/10.1002/aja.1001670405>.
 25. Haraguchi, H., Saito-Fujita, T., Hirota, Y., Egashira, M., Matsumoto, L., Matsuo, M., Hiraoka, T., Koga, K., Yamauchi, N., Fukayama, M., et al. (2014). MicroRNA-200a locally attenuates progesterone signaling in the cervix, preventing embryo implantation. *Mol. Endocrinol.* 28, 1108–1117. <https://doi.org/10.1210/me.2014-1097>.
 26. Cooley, A., Madhukaran, S., Stroebele, E., Colon Caraballo, M., Wang, L., Akgul, Y., Hon, G.C., and Mahendroo, M. (2023). Dynamic states of cervical epithelia during pregnancy and epithelial barrier disruption. *iScience* 26, 105953. <https://doi.org/10.1016/j.isci.2023.105953>.
 27. Lupu, I.E., Redpath, A.N., and Smart, N. (2020). Spatiotemporal Analysis Reveals Overlap of Key Proepicardial Markers in the Developing Murine Heart. *Stem Cell Rep.* 14, 770–787. <https://doi.org/10.1016/j.stemcr.2020.04.002>.
 28. Sountoulidis, A., Liontos, A., Nguyen, H.P., Firsova, A.B., Fysikopoulos, A., Qian, X., Seeger, W., Sundström, E., Nilsson, M., and Samakovlis, C. (2020). SCRINSHOT enables spatial mapping of cell states in tissue sections with single-cell resolution. *PLoS Biol.* 18, e3000675. <https://doi.org/10.1371/journal.pbio.3000675>.
 29. Deng, W.B., Liang, X.H., Liu, J.L., and Yang, Z.M. (2014). Regulation and Function of Deiodinases During Decidualization in Female Mice. *Endocrinology* 155, 2704–2717. <https://doi.org/10.1210/en.2014-1015>.
 30. Zheng, H.T., Fu, T., Zhang, H.Y., Yang, Z.S., Zheng, Z.H., and Yang, Z.M. (2020). Progesterone-regulated Hsd11b2 as a barrier to balance mouse uterine corticosterone. *J. Endocrinol.* 244, 177–187. <https://doi.org/10.1530/Joe-19-0349>.
 31. Bhurke, A.S., Bagchi, I.C., and Bagchi, M.K. (2016). Progesterone-Regulated Endometrial Factors Controlling Implantation. *Am. J. Reprod. Immunol.* 75, 237–245. <https://doi.org/10.1111/aji.12473>.
 32. Garcia-Flores, V., Romero, R., Peyvandipour, A., Galaz, J., Pusod, E., Panaitescu, B., Miller, D., Xu, Y., Tao, L., Liu, Z., et al. (2023). A single-cell atlas of murine reproductive tissues during preterm labor. *Cell Rep.* 42, 111846. <https://doi.org/10.1016/j.celrep.2022.111846>.
 33. Deng, W., Yuan, J., Cha, J., Sun, X., Bartos, A., Yagita, H., Hirota, Y., and Dey, S.K. (2019). Endothelial Cells in the Decidual Bed Are Potential Therapeutic Targets for Preterm Birth Prevention. *Cell Rep.* 27, 1755–1768.e4. <https://doi.org/10.1016/j.celrep.2019.04.049>.
 34. Kirkwood, P.M., Gibson, D.A., Smith, J.R., Wilson-Kanamori, J.R., Kelepouri, O., Esnal-Zufiaurre, A., Dobie, R., Henderson, N.C., and Saunders, P.T.K. (2021). Single-cell RNA sequencing redefines the mesenchymal cell landscape of mouse endometrium. *Faseb. J.* 35, e21285. <https://doi.org/10.1096/fj.202002123R>.
 35. Jiang, L., Sun, J., and Huang, D. (2022). Role of Slit/Robo Signaling pathway in Bone Metabolism. *Int. J. Biol. Sci.* 18, 1303–1312. <https://doi.org/10.7150/ijbs.66931>.
 36. Kim, B.J., Lee, Y.S., Lee, S.Y., Baek, W.Y., Choi, Y.J., Moon, S.A., Lee, S.H., Kim, J.E., Chang, E.J., Kim, E.Y., et al. (2018). Osteoclast-secreted SLIT3 coordinates bone resorption and formation. *J. Clin. Invest.* 128, 1429–1441. <https://doi.org/10.1172/JCI91086>.
 37. Rama, N., Dubrac, A., Mathivet, T., Ni Chárthaigh, R.A., Genet, G., Cristofaro, B., Pibouin-Fragner, L., Ma, L., Eichmann, A., and Chédotal, A. (2015). Slit2 signaling through Robo1 and Robo2 is required for retinal neovascularization. *Nat. Med.* 21, 483–491. <https://doi.org/10.1038/nm.3849>.
 38. Castro-Rivera, E., Ran, S., Thorpe, P., and Minna, J.D. (2004). Semaphorin 3B (SEMA3B) induces apoptosis in lung and breast cancer, whereas VEGF165 antagonizes this effect. *Proc. Natl. Acad. Sci. USA* 101, 11432–11437. <https://doi.org/10.1073/pnas.0403969101>.
 39. Pique-Regi, R., Romero, R., Garcia-Flores, V., Peyvandipour, A., Tarca, A.L., Pusod, E., Galaz, J., Miller, D., Bhatti, G., Para, R., et al. (2022). A single-cell atlas of the myometrium in human parturition. *JCI Insight* 7, e153921. <https://doi.org/10.1172/jci.insight.153921>.
 40. Renthal, N.E., Williams, K.C., and Mendelson, C.R. (2013). MicroRNAs—mediators of myometrial contractility during pregnancy and labour. *Nat. Rev. Endocrinol.* 9, 391–401. <https://doi.org/10.1038/nrendo.2013.96>.
 41. Bol, M., Wang, N., De Bock, M., Wacquier, B., Decrock, E., Gadicherla, A., Decaluwé, K., Vanheel, B., van Rijen, H.V.M., Krysko, D.V., et al. (2017). At the cross-point of connexins, calcium, and ATP: blocking hemichannels inhibits vasoconstriction of rat small mesenteric arteries. *Cardiovasc. Res.* 113, 195–206. <https://doi.org/10.1093/cvr/cwv215>.
 42. Hidema, S., Fukuda, T., Hiraoka, Y., Mizukami, H., Hayashi, R., Otsuka, A., Suzuki, S., Miyazaki, S., and Nishimori, K. (2016). Generation of Otr cDNA(HA)-Ires-Cre Mice for Gene Expression in an Oxytocin Receptor Specific Manner. *J. Cell. Biochem.* 117, 1099–1111. <https://doi.org/10.1002/jcb.25393>.
 43. Yu, J., Berga, S.L., Zou, W., Yook, D.G., Pan, J.C., Andrade, A.A., Zhao, L., Sidell, N., Bagchi, I.C., Bagchi, M.K., and Taylor, R.N. (2017). IL-1β Inhibits Connexin 43 and Disrupts Decidualization of Human Endometrial Stromal Cells Through ERK1/2 and p38 MAP Kinase. *Endocrinology* 158, 4270–4285. <https://doi.org/10.1210/en.2017-00495>.
 44. Matziari, M., Dive, V., and Yiotakis, A. (2007). Matrix metalloproteinase 11 (MMP-11; stromelysin-3) and synthetic inhibitors. *Med. Res. Rev.* 27, 528–552. <https://doi.org/10.1002/med.20066>.
 45. Kimura, A., Ohmichi, M., Takeda, T., Kurachi, H., Ikegami, H., Koike, K., Masuhara, K., Hayakawa, J., Kanzaki, T., Kobayashi, M., et al. (1999). Mitogen-activated protein kinase cascade is involved in endothelin-1-induced rat puerperal uterine contraction. *Endocrinology* 140, 722–731.
 46. Leiber, D., Banno, Y., and Tanfin, Z. (2007). Exogenous sphingosine 1-phosphate and sphingosine kinase activated by endothelin-1 induced myometrial contraction through differential mechanisms. *Am. J. Physiol. Cell Physiol.* 292, C240–C250.
 47. Fallerini, C., Daga, S., Benetti, E., Picchiotti, N., Zguro, K., Catapano, F., Baroni, V., Lanini, S., Bucalossi, A., Marotta, G., et al. (2021). SELP Asp603Asn and severe thrombosis in COVID-19 males. *J. Hematol. Oncol.* 14, 123. <https://doi.org/10.1186/s13045-021-01136-9>.
 48. Syed, S.M., Kumar, M., Ghosh, A., Tomasetig, F., Ali, A., Whan, R.M., Alterman, D., and Tanwar, P.S. (2020). Endometrial Axin2(+) Cells Drive Epithelial Homeostasis, Regeneration, and Cancer following Oncogenic Transformation. *Cell Stem Cell* 26, 64–80.e13. <https://doi.org/10.1016/j.stem.2019.11.012>.
 49. Sandman, C.A., Glynn, L., Schetter, C.D., Wadhwa, P., Garite, T., Chic-DeMet, A., and Hobel, C. (2006). Elevated maternal cortisol early in pregnancy predicts third trimester levels of placental corticotropin releasing hormone (CRH): priming the placental clock. *Peptides* 27, 1457–1463. <https://doi.org/10.1016/j.peptides.2005.10.002>.
 50. Elovitz, M.A., Gajer, P., Riis, V., Brown, A.G., Humphrys, M.S., Holm, J.B., and Ravel, J. (2019). Cervicovaginal microbiota and local immune response modulate the risk of spontaneous preterm delivery. *Nat. Commun.* 10, 1305. <https://doi.org/10.1038/s41467-019-09285-9>.
 51. Sakabe, N.J., Aneas, I., Knoblauch, N., Sobreira, D.R., Clark, N., Paz, C., Horth, C., Zifra, R., Kaur, H., Liu, X., et al. (2020). Transcriptome and regulatory maps of decidua-derived stromal cells inform gene discovery in preterm birth. *Sci. Adv.* 6, eabc8696. <https://doi.org/10.1126/sciadv.abc8696>.
 52. Gross, G.A., Imamura, T., Luedke, C., Vogt, S.K., Olson, L.M., Nelson, D.M., Sadovsky, Y., and Muglia, L.J. (1998). Opposing actions of prostaglandins and oxytocin determine the onset of murine labor. *Proc. Natl. Acad. Sci. USA* 95, 11875–11879. <https://doi.org/10.1073/pnas.95.20.11875>.
 53. Takayanagi, Y., Yoshida, M., Bielski, I.F., Ross, H.E., Kawamata, M., Onaka, T., Yanagisawa, T., Kimura, T., Matzuk, M.M., Young, L.J., and Nishimori, K. (2005). Pervasive social deficits, but normal parturition, in oxytocin receptor-deficient mice. *Proc. Natl. Acad. Sci. USA* 102, 16096–16101. <https://doi.org/10.1073/pnas.0505312102>.
 54. Rinaldi, S.F., Makiava, S., Saunders, P.T., Rossi, A.G., and Norman, J.E. (2017). Immune cell and transcriptomic analysis of the human decidua in term and preterm parturition. *Mol. Hum. Reprod.* 23, 708–724. <https://doi.org/10.1093/molehr/gax038>.
 55. Lim, H., Gupta, R.A., Ma, W.G., Paria, B.C., Moller, D.E., Morrow, J.D., DuBois, R.N., Trzaskos, J.M., and Dey, S.K. (1999). Cyclooxygenase-2-derived prostacyclin mediates embryo implantation in the mouse via PPARδ. *Genes Dev.* 13, 1561–1574. <https://doi.org/10.1101/gad.13.12.1561>.
 56. Yin, Y., Haller, M.E., Chadchan, S.B., Kommagani, R., and Ma, L. (2021). Signaling through retinoic acid receptors is essential for mammalian uterine receptivity and decidualization. *JCI Insight* 6, e150254. <https://doi.org/10.1172/jci.insight.150254>.

57. Manuck, T.A., Lai, Y., Ru, H., Glover, A.V., Rager, J.E., Fry, R.C., and Lu, K. (2021). Metabolites from midtrimester plasma of pregnant patients at high risk for preterm birth. *Am. J. Obstet. Gynecol. MFM* 3, 100393. <https://doi.org/10.1016/j.ajogmf.2021.100393>.
58. Bastos Maia, S., Rolland Souza, A.S., Costa Caminha, M.d.F., Lins da Silva, S., Callou Cruz, R.d.S.B.L., Carvalho Dos Santos, C., and Batista Filho, M. (2019). Vitamin A and Pregnancy: A Narrative Review. *Nutrients* 11, 681. <https://doi.org/10.3390/nu11030681>.
59. You, Y.A., Hwang, S.Y., Kim, S.M., Park, S., Lee, G.I., Park, S., Ansari, A., Lee, J., Kwon, Y., and Kim, Y.J. (2021). Identification of Indicators for Preterm Birth Using Retinoid Metabolites. *Metabolites* 11, 443. <https://doi.org/10.3390/metabo11070443>.
60. Jauniaux, E., Jurkovic, D., Hussein, A.M., and Burton, G.J. (2022). New insights into the etiopathology of placenta accreta spectrum. *Am. J. Obstet. Gynecol.* 227, 384–391. <https://doi.org/10.1016/j.ajog.2022.02.038>.
61. Salamonsen, L.A. (2003). Tissue injury and repair in the female human reproductive tract. *Reproduction* 125, 301–311. <https://doi.org/10.1530/rep.0.1250301>.
62. Evans, J., and Salamonsen, L.A. (2014). Decidualized human endometrial stromal cells are sensors of hormone withdrawal in the menstrual inflammatory cascade. *Biol. Reprod.* 90, 14. <https://doi.org/10.1095/biolreprod.113.108175>.
63. Thomas, V.G. (2019). The Link Between Human Menstruation and Placental Delivery: A Novel Evolutionary Interpretation: Menstruation and fetal placental detachment share common evolved physiological processes dependent on progesterone withdrawal. *Bioessays* 41, e1800232. <https://doi.org/10.1002/bies.201800232>.
64. Nagase, H., Visse, R., and Murphy, G. (2006). Structure and function of matrix metalloproteinases and TIMPs. *Cardiovasc. Res.* 69, 562–573. <https://doi.org/10.1016/j.cardiores.2005.12.002>.
65. Zhang, X., and Nothnick, W.B. (2005). The role and regulation of the uterine matrix metalloproteinase system in menstruating and non-menstruating species. *Front. Biosci.* 10, 353–366. <https://doi.org/10.2741/1533>.
66. Sternlicht, M.D., and Werb, Z. (2001). How matrix metalloproteinases regulate cell behavior. *Annu. Rev. Cell Dev. Biol.* 17, 463–516. <https://doi.org/10.1146/annurev.cellbio.17.1.463>.
67. Zhang, X., Huang, S., Guo, J., Zhou, L., You, L., Zhang, T., and Zhao, Y. (2016). Insights into the distinct roles of MMP-11 in tumor biology and future therapeutics (Review). *Int. J. Oncol.* 48, 1783–1793. <https://doi.org/10.3892/ijo.2016.3400>.
68. Matsushita, H., Hijioka, M., Hisatsune, A., Isohama, Y., Shudo, K., and Katsuki, H. (2012). Natural and synthetic retinoids afford therapeutic effects on intracerebral hemorrhage in mice. *Eur. J. Pharmacol.* 683, 125–131. <https://doi.org/10.1016/j.ejphar.2012.03.023>.
69. Niu, X., Wang, H., Zhao, L., Lian, P., Bai, Y., Li, J., and Qiao, J. (2022). All-trans retinoic acid increases the pathogenicity of the H9N2 influenza virus in mice. *Virology* 19, 113. <https://doi.org/10.1186/s12985-022-01809-y>.
70. Xue, R., Zhang, Q., Cao, Q., Kong, R., Xiang, X., Liu, H., Feng, M., Wang, F., Cheng, J., Li, Z., et al. (2022). Liver tumour immune microenvironment subtypes and neutrophil heterogeneity. *Nature* 612, 141–147. <https://doi.org/10.1038/s41586-022-05400-x>.
71. Guo, D.L., Wang, Z.G., Pei, M.S., Guo, L.L., and Yu, Y.H. (2020). Transcriptome analysis reveals mechanism of early ripening in Kyoho grape with hydrogen peroxide treatment. *BMC Genom.* 21, 784. <https://doi.org/10.1186/s12864-020-07180-y>.

STAR★METHODS

KEY RESOURCES TABLE

REAGENT or RESOURCE	SOURCE	IDENTIFIER
<i>Antibodies</i>		
Rat anti-CD45	BD Pharmingen	Cat# 553081 RRID:AB_394611
Rat anti-F4/80	eBioscience	Cat# 53480182 RRID:AB_469915
Rat anti-CD31	eBioscience	Cat# 11031185 RRID:AB_465013
Mouse anti-NK-1.1	BioLegend	Cat# 108705 RRID:AB_313392
Rabbit anti-H3K4me3	Abcam	Cat# ab8580 RRID:AB_306649
Rabbit anti-H3K4me1	Abcam	Cat# ab8895 RRID:AB_306847
Rabbit anti-H3K27me3	Diagenode	Cat# C15410069 RRID:AB_2814977
Rabbit anti-H3K27Ac	Active Motif	Cat# 39133 RRID:AB_2561016
Rabbit anti-IgG	Cell Signaling Technology	Cat# 3900 RRID:AB_1550038
Rat anti-PECAM1	Santa Cruz Biotechnology	Cat# sc-18916 RRID:AB_627028
Rabbit anti- α -SMA	Cell Signaling Technology	Cat# 19245 RRID:AB_2734735
Rabbit anti-LYVE-1	Cell Signaling Technology	Cat# 67538s
Rabbit anti-PR	Cell Signaling Technology	Cat# 8757S RRID:AB_2797144
Rabbit anti-ERa	Santa Cruz Biotechnology	Cat# sc-542 RRID:AB_631470
Rabbit anti-WT1	Proteintech	Cat# 12609-1-AP RRID:AB_2216225
Rabbit anti-HAND2	Abcam	Cat# Ab200040 RRID:AB_2923502
DBA-lectin	ZSGB-BIO	Cat# ZLI-9018
Rabbit anti-F4/80	Cell Signaling Technology	Cat# 30325 RRID:AB_2798990
Rat anti-CK8	DSHB	Cat# AB_531826 RRID:AB_531826
Fluorescein labeled Dolichos Biflorus Agglutinin (DBA)	Vectorlabs	FL-1031-2
Cy3 AffiniPure Donkey Anti-Rat IgG (H+L)	Jackson ImmunoResearch	Cat# 712-165-150 RRID:AB_2340666
Alexa Fluor® 594 AffiniPure Donkey Anti-Rabbit IgG (H+L)	Jackson ImmunoResearch	Cat# 711-585-152 RRID:AB_2340621
Alexa Fluor® 488 AffiniPure Donkey Anti-Rabbit IgG (H+L)	Jackson ImmunoResearch	Cat# 711-545-152 RRID:AB_2313584
Cy2 AffiniPure Donkey Anti-Rat IgG (H+L)	Jackson ImmunoResearch	Cat# 712-225-153 RRID:AB_2340674

(Continued on next page)

Continued

REAGENT or RESOURCE	SOURCE	IDENTIFIER
Chemicals, peptides, and recombinant proteins		
Collagenase I	Worthington	LS004196
Collagenase V	Worthington	LS004188
HBSS	Sigma-Aldrich	Cat#7447407
Dulbecco's Phosphate Buffered Saline	Sigma-Aldrich	D8537
PrimeScript™ RT reagent Kit with gDNA Eraser (Perfect Real Time)	TaKaRa	RR047A
TB Green® Premix Ex Taq™ II (Tli RNase H Plus)	TaKaRa	RR820Bii
cOmplete™, EDTA-free Protease Inhibitor Cocktail	Roche	04693132001
16% Formaldehyde	Cell Signaling Technology	12606S
Triton X-100	Sigma-Aldrich	T8787
SplintR® Ligase	NEB	M0375L
Phi29 MAX DNA Polymerase	Vazyme	N106-02
Retinoic acid	Med Chem Express	HY-14649
Deposited data		
Data of Cut & Tag assays and scRNA-Seq for days 16 and 19 deciduae	This study	PRJNA907416
Experimental models: Organisms/strains		
Mouse: CD1	TengXin Biotechnology	N/A
Software and algorithms		
Bowtie2(2.5.0)	Langmead and Salzberg, 2012	http://bowtie-bio.sourceforge.net/bowtie2/index.shtml
MACS2(2.2.7.1)	Zhang et al., 2008	https://github.com/taoliu/MACS
Seurat (4.3.0)	Hao et al., 2021	https://github.com/satijalab/seurat
CellphoneDB(v4)	Efremova et al., 2021	https://github.com/Teichlab/cellphonedb
Cellchat(1.5.0)	Suoqin et al., 2021	https://github.com/sqjin/CellChat
NicheNet (1.1.1)	Browaeys et al., 2019	https://github.com/saeyslab/nichenetr
TopHat2 (2.1.1)	Kim et al., 2013	https://ccb.jhu.edu/software/tophat/index.shtml
GraphPad Prism (8.0.0)	GraphPad	https://www.graphpad.com/scientific-software/prism/
Other		
Original code for data analysis applied in this paper.	This paper	https://doi.org/10.5281/zenodo.8275380
Accession number of original sequencing data	This paper	PRJNA907416

RESOURCE AVAILABILITY

Lead contact

Further information and requests for reagents and dataset may be directed to, and will be fulfilled by the Lead Contact, Wenbo Deng (wbdeng@xmu.edu.cn).

Material availability

All materials in this study will be made available on request to the [lead contact](#).

Data and code availability

- Single-cell RNA-seq and Cut & Tag data have been deposited at National Center for Biotechnology Information Sequence Read Archive and are publicly available as of the date of publication. Accession numbers are listed in the [key resources table](#).

- All original code has been deposited at Zenodo and is publicly available as of the date of publication. DOI is listed in the [key resources table](#).
- Any additional information required to reanalyze the data reported in this paper is available from the [lead contact](#) upon request.

EXPERIMENTAL MODEL AND SUBJECT DETAILS

Animals

Experiments were performed in 6~8 weeks female CD1 mice (purchased from TengXin Biotechnology, Chong Qing, China). Mice were housed in animal care facility of Xiamen University, which contained a controlled environment ($22 \pm 2^\circ\text{C}$, 50–60% humidity, 12-h light-dark cycles) and free access to food and water according to the guidelines for the care and use of laboratory animals. All experimental procedures were approved by the Animal Welfare Committee of Research Organization (X200811), Xiamen University. Maternal deciduae were collected on days 16 and 19, separately. The day of vaginal plug formation was considered Day 1 of pregnancy.

For atRA injection, pregnant mice were injected with atRA on days 16 and 17 with twice/day (800 $\mu\text{g}/\text{mouse}/\text{time}$).^{68,69} Mice parturition before day 19 morning was identified as accelerating the timing of parturition.

METHOD DETAILS

10x genomics single-cell RNA-seq of decidua tissue

The deciduae containing only maternal tissue from three individual on days 16 and 19 were surgically removed, mixed together, rinsed with ice-cold DPBS (Merck Millipore, D8537) and chopped using scalpels into small pieces and enzymatically digested in 5 mL digestion solution containing 1 mg/mL collagenase I (Worthington, LS004196) and 1 mg/mL collagenase V (Worthington, LS004188) in HBSS. The supernatant was diluted with HBSS and passed through 70- μm cell sieve and then 40- μm cell sieve (Biosharp, BS-40-CS). The flow-through was centrifuged and resuspended in 1 mL of red blood cell lysis buffer for 3 min. The cells were collected by spinning down at 500g for 5min and re-suspended in DPBS and kept on ice for subsequent 10X scRNA sequencing.

Flow cytometry staining and cell sorting

Decidual stromal cells were dissociated according to the protocol used before and incubated at 4°C for 30 min in 1ml FACS staining buffer (2% BSA in DPBS) with monoclonal antibodies specific to CD45 (BD Pharmingen, Cat# 553081) and CD31 (eBioscience, Cat#11031185). After removing CD45 positive immune cells and CD31 positive endothelial cells, the remaining CD45 and CD31 negative cells were purified for subsequent experiments, such as RNA seq and CUT&Tag. The antibodies used were listed in [key resources table](#).

Decidua stromal cell culture

Decidua stromal cells isolation followed the protocol as described before. Cells were plated in 12-wells plates containing phenol red-free Dulbecco modified Eagle medium (DMEM) and Ham F12 nutrient mixture (1:1) (Gibco) with 10% charcoal-stripped fetal bovine serum (CS-FBS) and antibiotic. Two hours later, the medium was replaced with fresh medium (DMEM/F12, 1:1) with 10% CS-FBS. After 24h culturing, the medium was replaced with DMEM/F12 without CS-FBS for 12h starvation. After 12h starvation, the medium was replaced with DMEM/F12 containing vehicle (DMSO) or atRA (5 μM) (MedChemExpress, HY-14649) for 24h.

CUT&Tag assay

The CUT&Tag assay was performed using the NovoNGS® CUT&Tag 3.0 High-Sensitivity Kit (NovoProtein, N259-YH01). In brief, 100,000 purified decidual stromal cells by FACS washed twice with 1.5 mL wash buffer and then mixed with 10 μL activated concanavalin A beads and incubated at RT for 10 min. After successive incubations with the primary antibody (overnight at 4°C) at a dilution of 1:50 and secondary antibody (room temperature, 1 h) at a dilution of 1:100, the cells were washed and incubated with 1 μL pAG-Tn5 in 100 μL ChiTag Buffer for 1 h at room temperature. Tagmentation buffer (50 μL) was added into the samples and incubated at 37°C for 1 h. The reaction was stopped by adding 1 μL 10% SDS and incubated at 55°C for 15 min. To extract DNA, 100 μL Tagment DNA extract beads were added to each tube with vortexing, quickly spun and held for 5 min. Tubes were placed on magnet stand, then the liquid was carefully withdrawn. Without disturbing the beads, beads were washed twice in 200 μL 80% ethanol. After drying for about 5 min, 37 μL of TE Buffer was added, the tubes were vortexed, quickly spun and allowed to sit for 3 min. Tubes were placed on a magnet stand and the liquid was transferred to a fresh tube.

Bulk RNA-Seq of decidual stromal cells

RNA was extracted from purified decidual stromal cells using TRIzol reagent (Vazyme, R401). RNA concentration was measured by NanoDrop (Thermo Fisher scientific, Waltham, MA) and the quality of RNA was determined by Agilent TapeStation 4200 (Agilent Technologies, Santa Clara, CA). Libraries were prepared using the TruSeq Stranded Total RNA Library Prep Kit (Illumina, San Diego, CA) from total RNA. Paired-end deep sequencing was done using HiSeq 2500 sequencer (Illumina, San Diego, CA).

RNA-seq data analysis

After alignment of the paired-end reads to mouse genome (GRCm38) by STAR with default parameters, gene expression was normalized to fragments per kilobase of exon model per million mapped reads (FPKM) using the EdgeR3.9 package in R with the criteria of fold change greater than 2 or less than 0.5 and $p < 0.05$. Ggplot2 package in R was applied for data visualization of RNA-Seq data. Gene ontology (GO) and KEGG enrichment analysis of differential expression genes (DEGs) were analyzed by clusterProfiler package in R.

Digoxigenin *In situ* hybridization (ISH)

In situ hybridization with digoxigenin (DIG) was modified according to the previously described method. Frozen sections (10 μm) were mounted onto poly-L-lysine coated slides and stored at -80°C until used. After removal from -80°C , the slides were placed on a slide warmer (37°C) for 3 min and then fixed in 4% paraformaldehyde in PBS for 60 min. Following prehybridization, sections were hybridized to DIG labeled cRNA probes overnight at 55°C . After hybridization, the slides were incubated with RNase A (10 mg/ml) at 37°C for 30 min. After incubated with alkaline phosphatase conjugated anti-Digoxigenin antibody (Fab fragments, Roche), the signal was visualized with 5-Bromo-4-chloro-3-indolyl phosphate (BCIP) and nitro blue tetrazolium (NBT). Primer pairs were listed in Table S1.

Single-molecule fluorescence *in situ* hybridization (ISS)

The padlock probes of genes of interesting were designed by PrimerQuest (<https://eu.idtdna.com/PrimerQuest/Home/Index?Display=AdvancedParams>). Tissue sections were removed from -80°C and mounted onto Superfrost Plus slides (ThermoFisher Scientific) at 45°C for 3 min, fixed in 4% PFA (freshly prepared) for 60 min. Blocking Master Mix containing tRNA and Oligo-dT was added and incubated the slides at room temperature (RT) for 30 min to block the unspecific binding of probes on the tissue section. Padlocks probes (0.5 μM each, listed in Table S2) were added and incubated at 55°C for 15 min for denaturation and at 45°C for 120 min for hybridization. SplintR ligase (PBCV-1 DNA Ligase, NEB, M0375L) was added to ligate the hybridized padlock probes for 12-16 hours at 25°C . Phi 29 (Φ 29) polymerase (Vazyme, N106-02) was added to perform the rolling circle amplification (RCA) at 30°C for 12-16 hours. After adding of detecting solution containing HRP-labeled detecting probes onto the slides and incubating in the dark for 45-60 min at RT, signal was visualized using TSA.

Immunofluorescence

The fresh tissue of whole implantation site of days 8, 10, 12, 14,16 and 19 were snap frozen in liquid nitrogen and then stored in -80°C . After embedded in OCT, the whole uteri of days 8, 10 and 12 were collected for immunofluorescence. For big tissue of day 14, 16 and 19, the fetus was trimmed off after embedded in OCT and the remaining maternal tissue of mesenterium (M) side was subjected to immunofluorescence. Briefly, tissue sections were fixed with 4% paraformaldehyde for 60 min, followed by three times washing in 0.1 % PBS-T (Sigma-Aldrich, T8787) for 5 min. Nonspecific binding was blocked with 5% BSA in PBS for 1h at room temperature. Tissue sections were then incubated with primary antibodies overnight at 4°C . Secondary antibodies and DAPI at a 1:200 dilution in 5% BSA were incubated for 1h at room temperature.

Quantitative real-time PCR

Total RNAs were extracted from decidual tissues or cells using TRIzol reagent (Vazyme, R401) according to the manufacturer's protocol, and 1 μg total RNA was utilized as template for reverse transcription to synthesize cDNA (TaKaRa , RR047A) according to the manufacturer's instructions. RT-qPCR was performed using TB Green™ Premix Ex Taq™ (TaKaRa , RR820B). Each experiment was repeated at least three times independently. Relative gene expression was analyzed using the delta delta CT method ($\Delta\Delta\text{CT}$). All RT-qPCR primer pairs were listed in Table S1.

Single cell RNA-seq data processing

Single-cell libraries were sequenced on Illumina HiSeq X Ten instruments using 150 bp paired-end sequencing. Reads were processed using the Cell Ranger 4.0.0 pipeline with the default and recommended parameters. This output was then imported into the Seurat (v3.0) R toolkit for quality control and downstream analysis of our single-cell RNA-seq data after batch correction by harmony package of R. All functions were run with default parameters unless specified otherwise. Low-quality cells (total UMI count per cell (library size) below 30,000, genes per cell < 500 and the content of mitochondria genes $> 20\%$) were excluded.⁷⁰ Next, we used a cluster-level approach to remove potential doublet cells. In brief, the doublet score was calculated for each cell using doubletCells function of R package v.1.18.7. There were totally 13,404 and 12,375 cells remained for day 16 and 19, respectively, for downstream analysis. Cell clusters in each sample were identified by examining the top 50 principal components (PCs) across highly variable genes (HVGs), building neighbour graph by buildSNNGraph function, and then clustering using the cluster_louvain function from the igraph R package v.1.2.9. The median doublet score of each cell cluster was calculated using median-centred MAD-variance normal distribution. Clusters with a median score above the extreme top end of this distribution were considered as doublets. After filtering, remaining cells were kept for the downstream analysis.

Cell clustering and annotation

A total of 2,000 HVGs were selected using the highly_variable_genes function, and then the top 50 PCs were calculated using the PCA function. We regressed out the effect of percentage of mitochondrial genes and scaled each gene to unit variance. Nearest neighbourhood graphs were built using the neighbours function, and the community algorithm was applied for clustering using the louvain function. The

dimensionality of each dataset was reduced using UMAP. The 25 major cells types identified in our dataset were annotated based on the well-known marker genes.

Gene-clustering analysis

After averaging expression of each gene in different cell types by AverageExpression function in Seurat, the genes expressed in Str_0, Str_1 and Str_2 was clustered into different groups depended on their expression patterns by TCGSeq R packag.⁷¹ Then, genes highly expressed in Str_0, Str_1 and Str_2 were subjected into KEGG analysis.

Calculation of gene signature scores based on scRNA-seq data

Gene signature scores of pluripotency and WNT signaling were calculated on the basis of the scRNA-seq data. For each gene signature, individual cells were scored using the AddModuleScore function, which calculated the average expression levels of selected genes at the single-cell level and subtracted by the aggregated expression of control feature sets which composed of 100 randomly selected genes' averaged expression.

Cell-cell interactions analysis by CellPhoneDB

To investigate potential interactions across different cell types in decidua, cell-cell interaction analysis was performed using CellPhoneDB, a public database that stores receptors, ligands, and their interactions.¹⁶ Both ligands and receptors included subunit structures that accurately represent heteromeric complexes. In brief, a log₂-normalized count matrix was subsampled into 500 cells per cluster. Significant ligand-receptor pairs were identified after filtering. For each ligand-receptor pair, the total number of this ligand-receptor pairs across clusters from the same cellular module was counted. Cellular-module-specific ligand-receptor pairs were then determined based on the enrichment score. To identify potential ligands that drive the latent phenotype, NicheNet (v.1.1.0) was applied to interrogate possible interaction and target genes between indicated cell types.

CellChat analysis of cell-cell communication

To further analyze and compare the intercellular communication differences between days 16 and 19 decidua, CellChat, an open-source R package (<https://github.com/sqjin/CellChat>) was used for scRNA-seq data. A database of signaling molecular interactions existed in this package, consisting of 60% of paracrine/autocrine signaling interactions, 21% of extracellular matrix (ECM)-receptor interactions and 19% of cell-cell contact interactions. Quantification of intercellular interactions was calculated based on differential expression of ligand-receptor pairs.

RNA velocity analysis

Read annotations for samples were performed using the velocity.py (v0.17.17) command-line tool (velocity run10x) with BAM, genome annotation, and repeat annotation files. The BAM file was produced by the default parameters of the Cellranger software (10x Genomics). The genome annotations GRCm38 from the Cellranger pre-built references were used to count molecules while separating them into three categories: 'spliced', 'unspliced', or 'ambiguous'. Repeat annotation files were downloaded from the UCSC genome browser. The velocity.R package v0.6 was used to calculate RNA velocity values for selected genes from each cell, and highly variably expressed genes computed by FindVariableFeatures function of Seurat were further filtered out based on a cluster-wise expression, then the remaining highly variably expressed genes were the selected genes as the input for velocity.R. Finally, The RNA velocity vectors were embedded to the UMAP plot produced by the Seurat R package.

Statistical analysis

Statistical analyses were performed using GraphPad Prism (v.9.0) (for experimental data), R (v.4.1.0) and RStudio (2021.09.1). Comparisons between groups were conducted using Student's t-tests and Wilcoxon rank-sum tests and ANOVA were used for continuous variables. $P < 0.05$ was considered to be statistically significant. No statistical methods were used to predetermine the sample size of scRNA-seq libraries. Unless otherwise noted, each experiment was repeated three or more times with biologically independent samples.